Impact demagnetization of the Martian crust: Current knowledge and future directions

Impact Demagnetization of the Martian Crust: Current Knowledge and Future Directions

Karin L. Louzada[1]*, Sarah T. Stewart[1], Benjamin P. Weiss[2], Jérôme Gattacceca[3], Robert J. Lillis[4], and Jasper S. Halekas[4]

[1]Department of Earth and Planetary Sciences, Harvard University, 20 Oxford Street, Cambridge, MA 02138, USA

[2]Department of Earth, Atmospheric and Planetary Sciences, Massachusetts Institute of Technology 54-814, 77 Massachusetts Avenue, Cambridge, MA 02139, USA

[3]Department of Geophysics and Planetology, CEREGE (CNRS, Aix-Marseille University), BP 80, 13545 Aix en Provence Cedex 4, France

[4]Space Sciences Laboratory, University of California, Berkeley, 7 Gauss Way, Berkeley, CA 94720-7450, USA

*louzada@post.harvard.edu

Submitted to EPSL Frontiers – August 19, 2009

Revised – September 26, 2010

Revised – February 27, 2011

Abstract

The paleomagnetism of the Martian crust has important implications for the history of the dynamo, the intensity of the ancient magnetic field, and the composition of the crust. Modification of crustal magnetization by impact cratering is evident from the observed lack of a measurable crustal field (at spacecraft altitude) within the youngest large impact basins (e.g., Hellas, Argyre and Isidis). It is hoped that comparisons of the magnetic intensity over impact structures, forward modeling of subsurface magnetization, and experimental results of pressure-induced demagnetization of rocks and minerals will provide constraints on the primary magnetic mineralogy in the Martian crust. Such an effort requires: (i) accurate knowledge of the spatial distribution of the shock pressures around impact basins, (ii) crustal magnetic intensity maps of adequate resolution over impact structures, and (iii) determination of demagnetization properties for individual rocks and minerals under compression. In this work, we evaluate the current understanding of these three conditions and compile the available experimental pressure demagnetization data on samples bearing (titano-) magnetite, (titano-) hematite, and pyrrhotite. We find that all samples demagnetize substantially at pressures of a few GPa and that the available data support significant modification of the crustal magnetic field from both large and small impact events. However, the amount of demagnetization with applied pressure does not vary significantly among the possible carrier phases. Therefore, the presence of individual mineral phases on Mars cannot be determined from azimuthally averaged demagnetization profiles over impact basins at present. The identification of magnetic mineralogy on Mars will require more data on pressure demagnetization of thermoremanent magnetization and forward modeling of the crustal field subject to a range of plausible initial field and demagnetization patterns.

44 keywords: Mars, paleomagnetism, impact cratering, pressure demagnetization, magnetic minerals

45

1. Introduction

1.1. The Martian magnetic field

Renewed interested in the Martian magnetic field has been fueled by detailed mapping by NASA's Mars Global Surveyor (MGS) spacecraft (Albee, et al., 2001) from 1997 to 2006. The Magnetometer (MAG) and Electron Reflectometer (ER) aboard MGS mapped the global crustal magnetic field at about 400 and 185 km altitude, respectively (see Figure 1). Although Mars currently does not possess a global magnetic field of internal origin stronger than 0.5 nT at the surface, intense localized magnetic fields of crustal origin (e.g., Acuña, et al., 1999; Lillis, et al., 2008) and remanent magnetization* in the Martian meteorite ALH 84001 (e.g., Weiss, et al., 2008) indicate that a substantial global field must have existed early in the planet's history. The distribution of the magnetic anomalies has been the subject of much debate as it is believed to have major implications for the ancient dynamo on Mars and the formation of the Martian crust.

The strongest magnetic anomalies are primarily located in the Noachian crust (>4 Ga) of the southern hemisphere. The observed crustal magnetic field is in some locations ~20 times greater than terrestrial magnetic anomalies at similar altitude, implying remanent magnetization of tens of A/m (Acuña, et al., 2001; Langel, et al., 1982). Such high intensities may be due to thermoremanent magnetization acquired as the crust cooled below the blocking temperatures* of the constituent ferromagnetic minerals, post-impact heating within large craters, and/or heating by magmatic intrusions (Arkani-Hamed, 2003; Arkani-Hamed, 2005; Hood, et al., 2007; McEnroe, et al., 2004). Many questions regarding the origin of the magnetization remain open. For example, the interpretation of quasi-parallel lineations of alternating magnetic polarity at

spacecraft altitude remains controversial (e.g., Connerney, et al., 2005; Harrison, 2000; Hood, et al., 2007).

1.2. Impact cratering and demagnetization processes

Another important observation is that impact cratering appears to have shaped large regions of the crustal magnetic field. The younger (<4.1 Ga, Frey, 2008) impact basins, Hellas (2070 km diameter), Argyre (1315 km) and Isidis (1352 km) are devoid of magnetic anomalies (Figure 1) because the crust has presumably been demagnetized by these impacts (e.g., Acuña, et al., 1999). In order to quantify how impacts have modified the crustal field, we must first understand impact-related demagnetization and remagnetization processes (Figure 2).

Impacts result in the excavation of magnetized crust from the crater cavity and act to redistribute material onto the surrounding terrain. Near the crater rim, the ejected material may be partially intact and folded; in the distal ejecta blanket however, the crustal material randomly deposited (Louzada, et al., 2008), which would not contribute to the observed magnetic intensity at altitude. Additionally, near the impact point, the impact energy is high enough to melt or vaporize the crust, destroying any primary magnetic remanence in the rocks. The resulting melt sheet that lines the crater floor will acquire a new thermoremanent magnetization in the ambient magnetic field upon cooling. If there is a very weak or nonexistent ambient field, the melt sheet will remain essentially unmagnetized.

With increasing distance from the impact point, r, shock pressures (and temperatures) decrease as $1/r^{1.5}$ to $1/r^{3}$ (the decay exponent depends on the impact velocity and material, Melosh, 1989, p. 62; Pierazzo, et al., 1997). Beyond the crater rim, where the shock has decayed to below a few GPa, the stress wave is elastic and pressure decreases as $1/r$. Nevertheless, in this region, shock heating is no longer substantial enough to affect the magnetic remanence of the

rocks. In the absence of a magnetic field, the low pressures (≤ a few GPa) found at this distance are known to demagnetize rocks and minerals (e.g., Borradaile, 1993; Borradaile and Jackson, 1993; Kinoshita, 1968; Nagata, 1971; Ohnaka and Kinoshita, 1968). In the presence of an ambient field, compression at low pressures results in the acquisition of shock remanent magnetization (SRM, e.g., Fuller, 1977; Gattacceca, et al., 2010; Gattacceca, et al., 2007; Srnka, et al., 1979). It has also been shown experimentally that impacts can generate or amplify ambient magnetic fields (Crawford and Schultz, 1993; Crawford and Schultz, 1999) capable of producing a strong SRM in shocked materials. However, at present, there is no evidence for shock related magnetic fields from terrestrial crater studies in basaltic rock (Louzada, et al., 2008; Weiss, et al., 2010). Nonetheless, the efficiency of SRM is typically several times less than that of thermoremanent magnetization. It is also more susceptible to viscous decay and may not be stable over geologic time (Gattacceca, et al., 2007). Finally, post-impact magnetic modification of the Martian crust could have occurred during hydrothermal metamorphism that may (e.g., Barnhart and Travis, 2010) or may not (e.g., Scott and Fuller, 2004) be impact related.

1.3. Impact demagnetization signatures of the Martian basins

The absence of central magnetic anomalies over the youngest impact basins (Hellas, Isidis, Argyre, Utopia and the North Polar basin, see Figure 1) has been used to date the cessation of the Martian dynamo at about ~4 Ga (Acuña, et al., 1999; Arkani-Hamed, 2004; Lillis, et al., 2008). This interpretation is based on the assumptions that melt sheets in these basins would have acquired a thermoremanence in the presence of an ambient magnetic field and that the remanence would have persisted to the present-day. Alternatively, impact-related thermoremanence could have been demagnetized as a result of multiple subsequent impacts on the basin floor. However, the spatial distribution and rate of impacts onto Mars is not likely to

have been homogeneous and constant, resulting in incomplete demagnetization of the centers of the basins. Because variations in crustal magnetic fields measured from orbit originate from lateral gradients in magnetization (as opposed to absolute magnetization) and demagnetization appears to be complete in these basins, the extremely low crustal fields observed over the basins also imply that indeed no significant magnetization was acquired in their centers when they formed (Acuña, et al., 1999; Lillis, et al., 2008).

The older basins (e.g. Ares, Daedalia, Zephyria) are associated with moderate-to-strong crustal magnetic fields and likely formed before the dynamo ceased (Lillis, et al., 2008). The cumulative history of impact events has likely substantially demagnetized the upper ~10 km of the Noachian crust (Arkani-Hamed, 2003). Similarly, secondary impacts by the ballistic ejecta of basin-forming events will also have contributed to impact demagnetization of the upper crust around basins greater than ~500 km in diameter (Artemieva, et al., 2005). Hence, a Noachian melt sheet of a few km thick is likely to have been extensively modified by subsequent impact events. The crustal magnetic fields measured over the old basins are therefore probably due to deep seated, coherently magnetized bodies (Shahnas and Arkani-Hamed, 2007). Such bodies may originate from magmatic intrusions beneath the basins (Watters, et al., 2009), analogous to those of the Sudbury Igneous Complex on Earth (Deutsch, et al., 1995).

1.4. Using impact craters to probe the magnetic crust

Hood et al. (2003) first correlated estimates of shock pressure with magnetic field intensities over Martian impact basins and experimental pressure demagnetization of magnetic minerals. Their study laid out a framework whereby an understanding of impact-induced demagnetization could provide information about the magnetic properties of the Martian crust. In order to infer the magnetic properties of the Martian crust based on impact demagnetization (Figure 3), the

following information is required:

(i) accurate knowledge of the spatial distribution of the shock pressures around impact basins,

(ii) crustal magnetic intensity maps of adequate resolution over impact structures (including a way to relate field intensity to magnetization strength and direction), and

(iii) determination of demagnetization properties for individual rocks and minerals under compression.

In this paper, we critically examine the state of knowledge of these three topics and identify outstanding questions. We then compile the available pressure demagnetization data of rocks and minerals from the literature and evaluate the demagnetization trends of individual minerals. Finally we discuss the implications for the Martian crust.

2. The magnetic crust of Mars

2.1. Candidate magnetic mineralogy

Multiple magnetic minerals are likely present in different regions of the Martian crust. The list of potential candidate phases responsible for the magnetization includes single-domain* magnetite, single-domain pyrrhotite, and multidomain* hematite (e.g., Dunlop and Arkani-Hamed, 2005). We briefly discuss these minerals below.

Magnetite is the most common magnetic mineral in the Earth's crust and has one of the highest spontaneous magnetizations*. A high Curie temperature* (580°C) suggests that magnetic remanence in magnetite is stable to great depths in the ancient Martian crust. Magnetite is an important carrier of remanence in the Martian meteorite ALH 84001 (Antretter, et al., 2003;

Rochette, et al., 2005; Weiss, et al., 2002; 2002) and is the main ferromagnetic mineral in Martian dust as inferred from rover magnet experiments (Madsen, et al., 2009). Titanomagnetite, the dominant magnetic carrier in some nakhlites (a subclass of Martian meteorites) (Rochette, et al., 2001), has a lower spontaneous magnetization (~75% that of magnetite) and easily oxidizes to titanomaghemite. Both titanomagnetite and titanomaghemite have low Curie temperatures (150-300 °C) and may exsolve during cooling into intergrown (potentially single-domain) magnetite and ilmenite.

Single-domain pyrrhotite, with a low Curie temperature of 320 °C, has a spontaneous magnetization 20% that of magnetite. Pyrrhotite is a secondary magnetic phase in ALH84001 (Kirschvink, et al., 1997; Weiss, et al., 2000; Weiss, et al., 2002) and the primary magnetic mineral in the Fe-rich basaltic shergottites (Lorand, et al., 2005; Rochette, et al., 2005; 2001), another subclass of Martian meteorites and considered to be most representative of the bulk Martian crust (Longhi, et al., 1992; McSween and Treiman 1998). Based on thermal considerations (the depth to the Curie temperature), it is unlikely that pyrrhotite is responsible for deep-seated magnetization on Mars, although it may be a contributing carrier in the shallower crust (above ~30 km). There is no evidence for ferromagnetic sulfides in Martian dust (Madsen, et al., 2009).

The presence of single-domain hematite (Curie temperature of 675 °C) on Mars has been inferred in Martian dust (Madsen, et al., 2009), and in rock coatings and spherules in outcrops (Klingelhöfer, et al., 2004). Although hematite dust and rock coverings are likely not responsible for large crustal magnetic anomalies, multidomain hematite could be a potential carrier on Mars if it was deep-seated and igneous in origin, as its thermoremanent potential is greater than that of single-domain hematite (although still a factor of 5 lower than that of single-domain magnetite)

(Dunlop and Kletetschka, 2001). Arkani-Hamed (2007) argues against coarse grained hematite as a carrier of intense magnetization as it would require unreasonably large amounts of hematite in the lower crust. Additionally, magnetization in low coercivity* phases such as multidomain hematite may not be stable over geologic time due to shock demagnetization (Dunlop and Arkani-Hamed, 2005; Gattacceca, et al., 2007).

2.2. Implications of the magnetic carrier on the magnetic crust

The identity of the magnetic carrier has implications for the thermal stability of crustal remanence as well as the oxidation state and chemistry of the crust. The presence of pyrrhotite at depth would indicate that the Martian crust was less oxidized than if magnetite were present. In situ observations of hematite and magnetite indicate higher oxidation levels at the surface. Magnetite, with its greater spontaneous magnetization, would require a lower concentration in the crust to explain the intensity of the field. The thickness of the Martian crust has been estimated to be around ~50 km with a crustal dichotomy in both thickness and magnetization (e.g., Nimmo and Tanaka, 2005). Estimates of the depth of the magnetic crust are strongly model dependent, and range from 30 to 50 km (Arkani-Hamed, 2003; Nimmo and Gilmore, 2001; Voorhies, 2008; Voorhies, et al., 2002). Maximum depths to Curie temperatures based on estimates of the ancient geothermal gradient for the Martian crust indicate that remanence in magnetite, hematite, and pyrrhotite are stable at depths down to 29-50 km, 33-70 km, and 13-35 km depth, respectively (e.g., Artemieva, et al., 2005; Dunlop and Arkani-Hamed, 2005; Nimmo and Gilmore, 2001). Over the past 4 Ga, lithostatic pressure and thermoviscous decay have decreased the magnetization in the lower crust, while impact demagnetization will have decreased it in the upper ~10 km of the crust (Shahnas and Arkani-Hamed, 2007).

3. A framework for interpreting shock demagnetization on Mars

3.1. Estimates of shock pressure around impact basins

It was quickly recognized that the shock pressures responsible for the demagnetization beyond ~1 crater radius from the center of large impact basins on Mars must have been only a few GPa (Hood, et al., 2003; Kletetschka, et al., 2004; Mohit and Arkani-Hamed, 2004). Using azimuthally averaged modeled magnetic intensities, Mohit and Arkani-Hamed (2004) estimated that complete demagnetization over Hellas basin occurs at distances up to 0.8 basin radii (present-day topographic basin radius ~1150 km), and that partial demagnetization extends out to ~1.2-1.4 basin radii, corresponding to radii of ~900 and ~1500 km, respectively.

Modeling of the shock pressure field around impact basins relies in part on the estimated projectile size and velocity. For a given crater diameter, scaling laws are used to estimate the size of the projectile, for an assumed impact velocity and density (rocky or icy). A two-step process relates (i) the impact conditions to the size of a transient crater (the hemispherical cavity that exists prior to gravitational collapse) and (ii) the transient cavity to the final observed crater size (after collapse). Geometric reconstructions of simple (bowl-shaped) and complex (e.g., central peak) craters provide constraints on the relationship between the transient and final crater size (for crater reconstructions see Melosh, 1989, p. 129 and 138). However, impact basins are morphologically very different from simple and complex craters, and their final geometries are not easily related to the volume of the transient cavity. For example, structural collapse and the development of multiple inward facing scarps (e.g., Argyre) may have destroyed the transient crater rim (Spudis, 1993, p.5, and references therein). Therefore, the final main topographic rim

of a basin does not represent the transient crater, as has been previously assumed (Hood, et al., 2003; Kletetschka, et al., 2004; Schultz and Frey, 1990). Additional complicating factors are extensive modification since formation (Tanaka and Leonard, 1995) and the ellipticity of all basins (Andrews-Hanna, et al., 2008). Computational techniques have only recently allowed for full numerical simulations of impact basin formation (e.g., Ivanov, et al., 2010).

Taking into account the uncertainties listed above, impactor radii of 125 to 342 km and impact velocities of 7.5 to 15 km/s have been invoked for the formation of Hellas (Hood, et al., 2003; Kletetschka, et al., 2004; Louzada and Stewart, 2009; Mohit and Arkani-Hamed, 2004). Initial pressure field estimates were made with the assumption that the planet's crust could be approximated as infinitely flat (after Melosh, 1984). However, Mars' small radius (3390 km) means that the curvature of the planetary surface results in a shallowing of the interference zone (the zone of reduced shock pressure near the surface, Figure 3) and higher shock pressures near the surface (Louzada and Stewart, 2009). Additionally, for large impacts, the presence of a density and sound-speed contrast at the crust-mantle boundary affects the propagation of the shock wave so that detailed near-surface pressure contours require numerical modeling of the impact event.

Figures 4 and 5 show the results of such a model for a 230 km and a 125 km radius projectile impacting at 9 km/s onto Mars (Louzada and Stewart, 2009). In the crust, the shock pressure contours are steeply inclined (nearly vertical, Figure 4). The averaged shock pressure with distance in the crust between 10 and 50 km depth is shown in Figure 5 (grey). If the demagnetization of magnetic minerals is sensitive to narrow pressure ranges, then steep pressure contours, in combination with magnetic intensity maps, may potentially be used to infer magnetic mineralogy.

For the 230 km radius impactor, at distances of ~900 and ~1500 km (corresponding to the radii of complete and partial demagnetization as inferred from magnetic field maps, respectively) the average shock pressures in the crust are 4.5 (± 1.0) and 1.5 (± 0.3) GPa, respectively. However, if the transient crater was much smaller than the main topographic rim of Hellas (e.g., if the scaling were closer to complex crater scaling), then the projectile may have been much smaller. In comparison, for a 125 km radius projectile, the inferred complete and partial demagnetization pressures are 1.3 (± 0.2) and 0.6 (± 0.1) GPa, respectively. Until we have a better understanding of impact basin formation and collapse, we will not be able to constrain the demagnetization shock pressures to better than a few GPa.

3.2. Crustal magnetic intensity over impact craters

The azimuthally averaged profile of the magnetic field intensity at 185 km altitude (Lillis, et al., 2008) (between 120° and 300° measured clockwise from geographic North) over Hellas basin is shown in Figure 5 (dark grey). The zone of near-zero magnetic field extends out to distances of 900-1000 km, beyond which its intensity increases smoothly and rapidly at distances up to 1400 km. Due to the highly non-unique relationship between subsurface magnetization and magnetic field measured from orbit, magnetic field data along single radial lines are not useful for constraining magnetization as a function of radius. Only by averaging over a wide range of azimuth angles does the general trend become clear. Azimuthally averaged radial profiles of the crustal magnetic field calculated from models of impact demagnetized crust can then be compared to azimuthally averaged magnetic field intensity data to constrain quantities such as average demagnetization radius. Lillis, et al. (2010) estimated this radius to be ~1300 km for Hellas basin.

Since the horizontal spatial resolution of magnetic maps from spacecraft observations is comparable to the orbital altitude (generally hundreds of km), detecting demagnetized craters in otherwise magnetized regions depends on the size of the crater, the coherence wavelength of the magnetization around the crater, and the altitude of observation. Magnetic field maps of Mars indicate a global average horizontal coherence wavelength of the crustal magnetization of ~650 to 1200 km. Because the crustal magnetic field strength decreases with altitude, magnetizations of such large wavelengths result in substantial masking of the magnetic signatures of demagnetized craters of length scales similar to the orbital altitude smaller than the horizontal coherence wavelength. Lillis, et al. (2010) estimated minimum demagnetized zone diameters capable of producing clear demagnetization signatures at 185 and 400 km altitude to be ~600 and ~1,000 km, respectively (or about ~2.5 times the observational altitude). Thus, from a statistical point of view, it is not surprising that the magnetic field maps do not display many dozens of circular holes over post-dynamo impact basins less than 1,000 km in diameter. Smaller impact craters could also produce magnetic signatures detectable at spacecraft altitude. However, it would not be possible to unambiguously conclude that these structures were impact demagnetized based solely on variations in magnetic intensity at altitude and additional constraints on the small-scale crustal magnetization would be needed.

Magnetic maps provide some additional constraints on the demagnetization of the crust. If the demagnetization was characterized by a region of zero magnetization surrounded by strong crustal remanence outside of the basin, then a magnetic edge effect would be observed at altitude (Figure 1 in Halekas, et al., 2009). The fact that this edge effect is not seen in magnetic maps and that the coherence scale is large suggests that the reduction in remanence is gradual in the radial direction from the basin center. Therefore, simple identification of a carrier phase with an

idealized pressure criterion for complete demagnetization will not be adequate. Instead, magnetic profiles must be modeled using the remaining remanence based on the shock pressure field. For very large impact basins, however, multiple overlapping craters and heterogeneity in the distribution of pre-impact crustal remanence may complicate the interpretation of the shock pressure history of the crust.

3.3. A thumbprint for shock demagnetization of rocks and minerals

Ideally, sensitivity of individual minerals to shock demagnetization would be sufficiently different to allow for unambiguous comparison with the magnetic field maps around impact basins. For example, the demagnetization of different minerals could occur in narrow pressure ranges that are distinct for each mineral or, hypothetically, minerals could demagnetize monotonically with applied shock pressure and reach complete demagnetization at very different pressure amplitudes. Recent experimental studies focused on static or dynamic pressure-induced demagnetization have been motivated by the desire to a have a mineral-specific pressure amplitude for complete demagnetization (e.g., Bezaeva, et al., 2007; Kletetschka, et al., 2004; Louzada, et al., 2007).

As discussed above, the inferred pressures for shock demagnetization on Mars based on the magnetic field maps are on the order of a few GPa. It has long been known that the remanence of magnetic materials is indeed permanently reduced as a result of compression in this pressure range (e.g., Cisowski and Fuller, 1978; Martin and Noel, 1988; Nagata, 1970; Pearce and Karson, 1981). In order to evaluate the uniqueness of the amplitude of pressure demagnetization of experimentally compressed rocks and minerals, we must first consider the differences between experimental procedures.

317 Neither dynamic nor static experiments can duplicate the exact conditions of planetary-scale
318 impact cratering. Dynamic experiments have a greater strain rate and shorter stress duration than
319 planetary-scale impact cratering, and the opposite holds for static experiments (Figure 6). If
320 kinetic processes play an important role in pressure demagnetization, then experiments
321 conducted under different conditions may not attain the same final results. In static experiments,
322 the greater efficiency of demagnetization in uniaxial loading compared to hydrostatic
323 compression has been attributed to greater shear stresses in the former (e.g., Martin and Noel,
324 1988).

325 Nagata (1971) and Pohl et al., (1975) found that the first application of a single mechanical
326 shock produces the greatest shock demagnetization effect and that repeated shocks have a
327 decreasing efficiency, asymptotically approaching a final remanence. The effect of hydrostatic
328 stress cycling on magnetic remanence is similar (Bezaeva, et al., 2007). Because pressure
329 demagnetization is often partially reversible upon decompression (0-15% in Bezaeva, et al.,
330 2007; Gilder and Le Goff, 2008), demagnetization measurements under pressure may slightly
331 overestimate the reduction in remanence.

332 The demagnetization observed in magnetic experiments is also dependent on the domain-size
333 and composition of the magnetic material (Bezaeva, et al., 2010) and its magnetic anisotropy
334 (Louzada, et al., 2010). It is also dependent on the type of magnetic remanence. High coercivity
335 remanence like thermoremanent magnetization is less susceptible to pressure demagnetization
336 than the saturation isothermal remanent magnetization* commonly used in pressure experiments
337 (Cisowski and Fuller, 1978).

338 In summary, as with the shock pressure distribution and magnetic field maps around impact
339 basins, the experimental data on pressure-induced demagnetization have caveats and limitations

in their application to impact demagnetization. Because the body of data on pressure-induced demagnetization has grown significantly in recent years, we next examine the data for different magnetic minerals to determine whether their responses to pressure are sufficiently different that they could be distinguished in the Martian crust using magnetic field maps of demagnetized impact basins.

4. A compilation of data on stress demagnetization

We have compiled the available experimental pressure demagnetization data on magnetite, titanomagnetite (Ti>40%), hematite, titanohematite, and pyrrhotite (Figure 7). We have included only single (first) applications of dynamic and static stress and all types of magnetization (isothermal, saturation isothermal, thermoremanent, and natural remanent magnetization). Based on the uncertainties in the shock pressures inferred at the edge of the demagnetized region around the Hellas basin (section 2.1), we focus on the 0 to 5 GPa pressure range. The studies included in the compilation are listed in Table 1. Additional experimental work not included in the compilation are experiments conducted at very low pressures (<~0.2 GPa) (Borradaile, 1992; Borradaile, 1992; 1993; Borradaile, 1994; Borradaile and Jackson, 1993; Borradaile and Mothershill, 1991; Carmichael, 1968; Graham, et al., 1957; Hamano, 1983; Martin and Noel, 1988; Nagata and Carleton, 1969; Shapiro and Ivanov, 1967; Stott and Stacey, 1960), shock experiments with uncertain pressure calibration (Cisowski and Fuller, 1978; Hargraves and Perkins, 1969), or explosive shock experiments on porous samples and/or accompanied by extensive heating (Kohout, et al., 2007; Pesonen, et al., 1997). Because it is not clear whether pressure studies on iron and iron-nickel alloys motivated by lunar studies are applicable to Mars, they have also been excluded (Bezaeva, et al., 2010; Dickinson and Wasilewski, 2000;

Wasilewski, 1976).

4.1. Magnetite

The low-pressure demagnetization behavior of magnetite (and low Ti magnetite, Ti <40%) up to 2 GPa is variable (Figure 7A), and there do not appear to be distinct differences between the single-domain and multidomain fractions. The demagnetization results appear to be very complicated. On average, however, the multidomain samples (blue symbols) are more demagnetized than the pseudo-single-domain* fractions (green symbols) at similar pressures. This result is consistent with multidomain magnetite having a lower coercivity and being more susceptible to pressure demagnetization than single-domain magnetite (Bezaeva, et al., 2010; Cisowski, et al., 1976; Cisowski and Fuller, 1978; Kletetschka, et al., 2004; Pearce and Karson, 1981), but not with the results from Gilder et al. (2006) who observe the opposite upon initial application of compression. Planar shock recovery experiments on single-domain magnetite bearing *Chiton stelleri* (a mollusk) teeth conducted in the Shock Compression Laboratory at Harvard attained complete demagnetization at 10 GPa (unpublished). However, Bezaeva, et al. (2010) find that remaining magnetization of magnetite and titanomagnetite, up to 1.24 GPa is dependent on the coercivity of the grains and is approximately proportional to $\ln(B_{cr})$, where B_{cr} is the coercivity of remanence*. Unfortunately, demagnetization data are not available in the critical 2-5 GPa range and it is likely that demagnetization trends will change when plastic deformation takes place. For example, brecciation will occur in rocks and minerals when the stress limit for elastic deformation has been exceeded. This limit, known as the Hugoniot Elastic Limit, is on the order of a few GPa in most rocks and minerals (Table 3.1 in Melosh, 1989; Sekine, et al., 2008). At present, there is no characteristic pressure for complete demagnetization for magnetite.

4.2. Titanomagnetite

More dynamic pressure demagnetization data exists for pseudo-single-domain titanomagnetite (Ti>40%) with saturation isothermal remanent magnetization up to ~4.5 GPa, and natural remanent magnetization up to 20 GPa. Natural and thermoremanent magnetization appear to be more resistant to pressure up to 5 GPa (Figure 7B) than saturation isothermal remanent magnetization in both the multidomain and pseudo-single domain samples. In titanomagnetite, magnetic remanence is more sensitive to shock compression in multidomain grains than it is in pseudo-single-domain grains at ~0.5 GPa (compare solid green and solid blue symbols in Figure 7B). However, in hydrostatic experiments (open symbols), the fraction of remanence in pseudo-single-domain and single-domain samples demagnetized at 1.24 GPa is variable (between 0.45 and 0.9). In titanomagnetite, pressure demagnetization is not only dependent on the domain state, but is also correlated with the Ti content of the mineral (Bezaeva, et al., 2010). Although explosive experiments on titanomagnetite-bearing basalt (solid green squares) resulted in a net decrease of magnetization, a shock remanent magnetization was simultaneously acquired in the terrestrial field and accounts for ~22% of the remaining magnetization at ~2 GPa. If corrected for this shock remanent magnetization, the trend would be shifted down (arrow in Figure 7B). The remaining offset of ~50% with the laser shock experiments (solid green diamonds) is probably a result of the lower susceptibility to demagnetization of natural (thermoremanent) magnetization with respect to saturation isothermal remanent magnetization, illustrating the importance of the initial coercivity distribution of the remanence carrying grains.

4.3. Hematite and Titanohematite

Only limited pressure demagnetization studies have been performed on SD hematite under hydrostatic pressures up to 1.24 GPa, and on multidomain hematite under dynamic pressure up to 4 GPa (Figure 7C). The fraction of remanence carried by multidomain hematite that is demagnetized at low pressures varies significantly (at ~1 GPa between 0.8 and 0.3 and a single measurement at 4 GPa indicates 0.4). No single domain pressure demagnetization data has been acquired above 1.24 GPa. Titanohematite has only been investigated in dynamic drop experiments on single-domain grains at about 1 GPa (Figure 7D). Although both minerals demagnetize as a result of pressure, it is not possible to extract a demagnetization trend from the available data.

4.4. Pyrrhotite

The demagnetization of single-domain, pseudo-single-domain and multidomain pyrrhotite has been studied in both planar impact shock experiments (up to 12 GPa) and in hydrostatic compression (up to 3 GPa) (Figure 7E; Figure 2B in Louzada, et al. (2010)). At low pressures (<3 GPa) saturation isothermal remanence of pyrrhotite demagnetizes similarly to saturation isothermal remanent magnetization in titanomagnetite (Figure 7B). At shock pressures above a transition to paramagnetism* (Rochette, et al., 2003) and the Hugoniot Elastic Limit (Louzada, et al., 2007; 2010) of pyrrhotite (both at ~3 GPa), demagnetization is partially counteracted by shock-induced changes in the magnetic properties of the material, consistent with an observed increase in single-domain like behavior. This observed stress hardening has also been noted in other materials (Gattacceca, et al., 2007; Gilder, et al., 2004; Jackson, et al., 1993).

5. Discussion

5.1. Generalizing the results

Despite the aforementioned difficulties in comparing the experimental results, we can draw some general conclusions regarding the effects of compression on the magnetic remanence of rocks and minerals at pressures below 5 GPa. Although the amount of demagnetization for a single mineral phase is highly variable, all minerals discussed demagnetize substantially at low pressures and the remaining magnetization decreases with increasing pressure. For example, below ~3 GPa, demagnetization trends for saturation isothermal remanent magnetization in titanomagnetite and pyrrhotite are remarkably similar (Figure 7B and E).

Significant scatter in the experimental results is due to differences in coercivity (domain size and type of remanence – saturation versus thermoremanent magnetization) and sample type (composition and pure mineral versus mineral bearing rocks) and prevents the extraction of detailed individual demagnetization trends from Figure 7. Regardless, at low pressures, the relative demagnetization differences between mineral phases are not sufficiently distinct so as to provide individual magnetic thumbprints (see also Bezaeva, et al., 2007).

Nevertheless, these data demonstrate that the estimated threshold for complete demagnetization of the Martian crust at a few GPa, as estimated from magnetic field maps and shock pressure distribution estimates around impact basins, is reasonable. Since the mechanical properties of rocks and minerals are similar, we do not expect substantially different demagnetization mechanisms to be occurring in different rocks and minerals. Mechanisms suggested to be responsible for stress demagnetization and shock demagnetization at pressures below the Hugoniot Elastic Limit are the effects of stress on magnetostriction (the spontaneous

change in shape of a crystal lattice as a result of magnetization and vice versa) (Gilder, et al., 2004; Kinoshita, 1968; Nagata, 1966). In larger grains, domain-wall displacement (Borradaile and Jackson, 1993; Nagata and Carleton, 1969) may also be an important demagnetization mechanism. Additionally, microbrecciation has been shown to have a profound effect on the domain structures of pyrrhotite in shock experiments (Louzada, et al., 2010) as well as in naturally shocked pyrrhotite-bearing rocks (Kontny, et al., 2007).

Similar deformation mechanisms are active during static and dynamic pressure experiments (e.g., dislocation generation and movement, microfracturing); however, the stress at which a material fails and the final demagnetization state attained can be different in static versus dynamic deformation because of differing strain rates and loading paths. The data presented here suggest that static and dynamic demagnetization is similar at low pressures (< several GPa). However, until static pressure techniques are developed that can expand the pressure range to complete demagnetization, we cannot conclusively state that full demagnetization occurs at the same dynamic and static pressure.

5.2. Naturally shocked rocks

Pressure demagnetization preferentially affects the lowest coercivity fractions in all rocks (Bezaeva, et al., 2007; Cisowski and Fuller, 1978; Gattacceca, et al., 2007; Jackson, et al., 1993; Louzada, et al., 2010). As the magnetization of the Martian crust is likely due to thermoremanent magnetization carried by grains with relatively high coercivity, the Martian crust will be less susceptible to demagnetization compared to most of the experimental samples. Additionally, caution should be taken when applying experimental results on pure minerals to planetary crusts. For example, above the Hugoniot Elastic Limit, the magnitude of demagnetization in pure pyrrhotite depends on the stress orientation with respect to the magnetic anisotropy whereas

474 less anisotropic pyrrhotite-bearing schists are not sensitive to stress orientation.

475 On planets with a global magnetic field, shock demagnetization may be partially
476 compensated for by the acquisition of shock remanent magnetization (Gattacceca, et al., 2007;
477 2007). The significance of transient impact-induced or amplified magnetic fields (Crawford and
478 Schultz, 1988; Martelli and Newton, 1977) is unclear as the magnetizing potential of these fields
479 is only located near the surface and their coherence scales are unknown. Additionally, shock-
480 related changes in magnetic remanence may be obscured by viscous processes. For example, at
481 Lonar crater, India (1.88 km diameter), titanomagnetite-bearing basalts shocked to a few GPa
482 contain a strong viscous remanent magnetic overprint acquired over the last 50 kyr since the
483 formation of the crater which obscures any potential evidence of shock effects on the
484 paleomagnetism of the rocks (Louzada, et al., 2008). Experiments indicate that the efficiency of
485 shock remanent acquisition is less than that of thermal remanence (≥17% for pseudo-single-
486 domain titanomagnetite bearing basalt, Gattacceca, et al., 2007) and that shock remanent
487 magnetization may be more susceptible to viscous decay. In addition, impact-generated fields
488 greater than several tens of μT were not detected at Lonar (Weiss, et al., 2010). For these
489 reasons, we assert that shock remanent magnetization can generally be neglected in the
490 interpretation of the Martian crustal field.

491 ### *5.3. Intensity of the Martian crustal magnetic field*

492 Perhaps the greatest outstanding question regarding the Martian crustal magnetic field is the
493 nature of the localized high intensities associated with certain areas of Noachian terrain (Acuña,
494 et al., 1999). Not only must the magnetic carrier phase(s) satisfy the observed low (several GPa)
495 pressure impact demagnetization, but they must also be able to carry strong magnetization and
496 retain that remanence over geologic time (~4 Gyr). Therefore, high magnetic intensities are

presumably due to thermoremanence acquired during emplacement of igneous rocks in a strong global magnetizing field and/or a high concentration of magnetic minerals. Estimates of the paleointensity of the Martian magnetic field based on the ~4 Ga meteorite ALH 84001 (e.g., Weiss, et al., 2008) and magnetostrophic balance considerations (Arkani-Hamed, 2005) are within an order of magnitude similar to (or less than) that of present-day Earth. If Martian basalts are enriched in Fe, then they possibly contain higher fractions of magnetic minerals, including pyrrhotite. Dunlop and Arkani-Hamed (2005) estimated that it would require 2 to 4 wt% of pyrrhotite in the Martian crust to explain the intense magnetization if the field strength was similar to that of the present-day Earth and the magnetization of the crust was similar to that of fresh mid-ocean ridge basalt. To date, the pyrrhotite content of basaltic shergottite meteorites has been found to be between 0.16 and 1.0 wt% (Rochette, et al., 2005). It has however been experimentally shown that synthetic Fe-rich Martian basalts rich in spinel-structured oxides are capable of acquiring intense thermoremanent magnetization (Bowles, et al., 2009). In any case, magnetic field intensity need not have been uniform on Mars (Stanley, et al., 2008). At present, a satisfactory mechanism for producing localized high magnetic intensities on Mars has not been developed.

5.4. Evaluation of the framework for shock demagnetization on Mars and future work

The first-order hypothesis that the Martian crust has been demagnetized by large basin-forming impacts is robust. The three components of the framework set out in section 1.6 consistently indicate that impact demagnetization on Mars occurred below 5 GPa. All magnetic minerals are effectively demagnetized in this pressure range, which is reasonable considering the similar mechanical properties of most rocks and minerals. Initial agreement between shock and

static experiment results suggest that both types of experiment yield results appropriate for studying planetary-scale impact cratering. However, because of the dependence of demagnetization on the initial coercivity distribution, more demagnetization data are needed on thermoremanent magnetization in rocks and minerals.

Static pressure experiments are presently limited by the maximum attainable hydrostatic pressure in the cell. Extrapolation of these results to greater pressures must be done with caution. Demagnetization trends versus pressure are likely to change as brecciation and defect generation become more important at pressures nearing the elastic limit. Inferred demagnetization pressures from the magnetic maps indicate that demagnetization occurs right at the cusp where permanent deformation of rocks and minerals takes place. More static pressure demagnetization experiments in the 2 to 5 GPa range and measurements of the Hugoniot Elastic Limit are desired for all the minerals discussed above.

More detailed interpretations of pressure demagnetization of the Martian crust are complicated by the degeneracy of the demagnetization data, limitations of the magnetic maps, and uncertainties in impact basin formation processes. In order to answer secondary questions regarding the magnetization of the crust (e.g., the coherence scale of magnetization, distribution of magnetic carrier phases, and magnetic mineralogy) more sophisticated forward modeling with hypothetical initial field and demagnetization patterns is required. This type of modeling is not trivial as the coherence scale of magnetization and the distribution of magnetic carriers may be codependent. However, it may help constrain the trend of remaining magnetization versus radius (or pressure) as a means of identifying magnetic carrier phases.

6. Conclusions

In this work, we postulated that in order to infer properties of the magnetized crust of Mars from observations of the magnetic field we need: (i) accurate estimates of the shock pressure distribution around impact basins, (ii) crustal magnetic intensity maps of adequate resolution over impact structures, and (iii) a unique thumbprint for the magnetic response of different rocks and minerals to compression. Detailed shock pressure contours in the crust require numerical simulations and cannot be easily approximated. Until we have a better understanding of how large impact craters and basins collapse, we will not be able to constrain (complete or partial) shock demagnetization pressures better than a few GPa.

However, even if the detailed demagnetization pressures from magnetic intensity maps and demagnetization trends from experimental results are lacking at present, the basic premise set out in the beginning of this paper still holds. A compilation of the available pressure demagnetization data of (titano-) magnetite, (titano-) hematite, and pyrrhotite, while considering the differences in experimental conditions (type of remanence, stress regime, mineralogy and grain-size), indicates a universal trend: all minerals demagnetize substantially (by several tens of percent) as a result of compression below 5 GPa. This behavior is probably due to the similar mechanical properties of the magnetic minerals and rocks. Individual demagnetization trends of magnetic minerals do not lend mineral specific thumbprints that can be mapped onto magnetic profiles over impact structures.

More detailed interpretations of impact demagnetization of the Martian crust require: (1) a better understanding of basin formation and collapse, (2) more pressure demagnetization data on thermoremanent magnetization in rocks and minerals, (3) more static and dynamic pressure demagnetization of rocks and minerals in overlapping pressure regimes up to 5 GPa (past the

565 Hugoniot Elastic Limit), and (4) forward modeling of the coherence scale of the magnetization,
566 distribution of magnetic carriers in the crust and magnetic crustal intensities on Mars.

567

568 **Acknowledgements**

569 Thanks to Natalia Bezaeva for providing a preprint of her manuscript. This research is
570 supported by NASA Mars Fundamental Research Program (NNG04GD17G, NNX07AQ69G,
571 and NNX06AD14G). K.L.L. was supported by the Amelia Earhart Fellowship (Zonta Int.). This
572 manuscript benefited greatly from the critical review by two anonymous reviewers.

573

574 **References**

575 Acuña, M.H., Connerney, J.E.P., Ness, N.F., Lin, R.P., Mitchell, D., Carlson, C.W., McFadden,
576 J., Anderson, K.A., Rème, H., Mazelle, C., Vignes, D., Wasilewski, P., Cloutier, P., (1999).
577 Global Distribution of Crustal Magnetization Discovered by the Mars Global Surveyor
578 MAG/ER Experiment, Science 284, 790-793, doi:10.1126/science.284.5415.790.

579 Acuña, M.H., Connerney, J.E.P., Wasilewski, P., Lin, R.P., Mitchell, D., Anderson, K.A.,
580 Carlson, C.W., McFadden, J., Rème, H., Mazelle, C., Vignes, D., Bauer, S.J., Cloutier, P.,
581 Ness, N.F., (2001). Magnetic field of Mars: Summary of results from the aerobraking and
582 mapping orbits, JGR 106, 23403-23417, doi:10.1029/2000JE001404.

583 Albee, A.L., Arvidson, R.E., Palluconi, F., Thorpe, T., (2001). Overview of the Mars Global
584 Surveyor mission, JGR 106, 23291-23316, doi:10.1029/2000JE001306.

585 Andrews-Hanna, J.C., Zuber, M.T., Banerdt, W.B., (2008). The Borealis basin and the origin of
586 the martian crustal dichotomy, Nature 453, 1212-1215, doi:10.1038/nature07011.

587 Antretter, M., Fuller, M., Scott, E., Jackson, M., Moskowitz, B., Solheid, P., (2003).
588 Paleomagnetic record of Martian meteorite ALH84001, JGR 108,
589 doi:10.1029/2002JE001979.

590 Arkani-Hamed, J., (2003). Thermoremanent magnetization of the Martian lithosphere, JGR 108,
591 doi:10.1029/2003JE002049.

592 Arkani-Hamed, J., (2004). Timing of the Martian core dynamo, JGR 109,
593 doi:10.1029/2003JE002195.

594 Arkani-Hamed, J., (2005). Magnetic crust of Mars, JGR 110, doi:10.1029/2004JE002397.

595 Arkani-Hamed, J., (2005). On the possibility of single-domain/pseudo-single-domain magnetic
596 particles existing in the lower crust of Mars: Source of the strong magnetic anomalies, JGR
597 110, E12009, doi:10.1029/2005JE002535.

598 Arkani-Hamed, J., (2007). Magnetization of the Martian Lower Crust: Revisited, JGR 112,
599 doi:10.1029/2006JE002824.

600 Artemieva, N., Hood, L., Ivanov, B.A., (2005). Impact demagnetization of the Martian crust:
601 Primaries versus secondaries, GRL 32, doi:10.1029/2005GL024385.

602 Barnhart, C.J.N., Francis, Travis, B.J., (2010). Martian post-impact hydrothermal systems
603 incorporating freezing, Icarus 208, 101-117, doi:10.1016/j.icarus.2010.01.013.

604 Bezaeva, N.S., Gattacceca, J., Rochette, P., Sadykov, R.A., Trukhin, V.I., (2010).
605 Demagnetization of terrestrial and extraterrestrial rocks under hydrostatic pressure up to 1.2
606 GPa, PEPI 179, 7–20, doi:10.1016/j.pepi.2010.01.004.

607 Bezaeva, N.S., Rochette, P., Gattacceca, J., Sadykov, R.A., Trukhin, V.I., (2007). Pressure
608 demagnetization of the Martian crust: Ground truth from SNC meteorites, GRL 34, L23202,
609 doi:10.1029/2007GL031501.

610 Borradaile, G.J., (1992). Deformation of remanent magnetism in a synthetic aggregate with
611 hematite, Tectonophysics 206, 203-218, doi:10.1016/0040-1951(92)90377-I.

612 Borradaile, G.J., (1992). Experimental deformation of two-component IRM in magnetite-bearing
613 limestone: a model for the behaviour of NRM during natural deformation, PEPI 70, 64-77,
614 doi:10.1016/0031-9201(92)90161-N.

615 Borradaile, G.J., (1993). Strain and magnetic remanence, Journal of Structural Geology 15, 383-
616 390, doi:10.1016/0191-8141(93)90134-V.

617 Borradaile, G.J., (1994). Remagnetisation of a rock analogue during experimental triaxial
618 deformation, PEPI 83, 147-163, doi:10.1016/0031-9201(94)90069-8.

619 Borradaile, G.J., Jackson, M., (1993). Changes in magnetic remanence during simulated deep
620 sedimentary burial, PEPI 77, 315-327, doi:10.1016/0031-9201(93)90106-J.

621 Borradaile, G.J., Mothershill, J.S., (1991). Experimental strain of isothermal remanent
622 magnetization in ductile sandstone, PEPI 65, 308-318, doi:10.1016/0031-9201(91)90137-7.

623 Boustie, M., Cottet, F., (1991). Experimental and numerical study of laser induced spallation into
624 aluminum and copper targets, Journal of Applied Physics 69, 7533-7538,
625 doi:10.1063/1.347570.

626 Bowles, J.A., Hammer, J.E., Brachfeld, S.A., (2009). Magnetic and petrologic characterization of
627 synthetic Martian basalts and implications for the surface magnetization of Mars, JGR 114,
628 E10003, doi:10.1029/2009JE003378.

629 Carmichael, R.S., (1968). Stress Control of Magnetization in Magnetite and Nickel, and
630 Implications for Rock Magnetism, J. Geomagn. Geoelectr. 20, 187-196.

631 Cisowski, S.M., Dunn, J.R., Fuller, M., Wu, Y., Rose, M.F., Wasilewski, P.J., (1976). Magnetic
632 effects of shock and their implications for lunar magnetism (II), Lunar Science Conference,
633 7th, Houston, Tex., March 15-19, 1976, Proceedings 3, 3299-3320.

634 Cisowski, S.M., Fuller, M., (1978). The Effect of Shock on the Magnetism of Terrestrial Rocks,
635 JGR 83, 3441-3458, doi:10.1029/JB083iB07p03441.

636 Connerney, J.E.P., Acuña, M.H., Ness, N.F., Kletetschka, G., Mitchell, D.L., Lin, R.P., Reme,
637 H., (2005). Tectonic implications of Mars crustal magnetism, Proceedings of the National
638 Academy of Sciences of the United States of America 102, doi:10.1073/pnas.0507469102.

639 Crawford, D.A., Schultz, P.H., (1988). Laboratory observations of impact-generated magnetic
640 fields, Nature 336, 50-52, doi:10.1038/336050a0.

641 Crawford, D.A., Schultz, P.H., (1993). The Production and Evolution of Impact-Generated
642 Magnetic Fields, Int. J. Impact Eng. 14, 205-216.

643 Crawford, D.A., Schultz, P.H., (1999). Electromagnetic Properties of Impact-Generated Plasma,
644 Vapor and Debris, Int. J. Impact Eng. 23, 169-180.

645 Deutsch, A., Grieve, R.A.F., Avermann, M., Bischoff, L., Brockmeyer, P., Buhl, D., Lakomy, R.,
646 Müller-Mohr, V., Ostermann, M., Stöffler, D., (1995). The Sudbury Structure (Ontario,
647 Canada): a tectonically deformed multi-ring impact basin, Iternational Journal of Earth
648 Sciences 84, 697-709, doi:10.1007/BF00240561.

649 Dickinson, T.L., Wasilewski, P., (2000). Shock Magnetism in Fine Particle Iron, MAPS 35, 65-
650 74, doi:10.1111/j.1945-5100.2000.tb01974.x.

651 Dunlop, D.J., Arkani-Hamed, J., (2005). Magnetic minerals in the Martian crust, JGR 110,
652 E12S04, doi:10.1029/2005JE002404.

653 Dunlop, D.J., Kletetschka, G., (2001). Multidomain Hematite: A Source of Planetary Magnetic
654 Anomalies? GRL 28, 3345-3348, doi:10.1029/2001GL013125.

655 Frey, H., (2008). Ages of very large impact basins on Mars: Implications for the late heavy
656 bombardment in the inner solar system, GRL 35, L13203, doi:10.1029/2008GL033515.

657 Fuller, M.D., (1977). Review of effects of shock (<60 kbar; $<6x10^9$ Pa) on magnetism of lunar
658 samples, Philosophical Transactions of the Royal Society of London. Series A, Mathematical
659 and Physical Sciences 285, 409-416, doi:10.1098/rsta.1977.0082.

660 Gattacceca, J., Berthe, L., Boustie, M., Vadeboin, F., Rochette, P., De Resseguier, T., (2007). On
661 the efficiency of shock remanent processes, PEPI doi:10.1016/j.pepi.2007.1009.1005.

662 Gattacceca, J., Boustie, M., Lima, E., de Resseguier, T., Cuq-Lelandais, J.P., (2010). Unraveling
663 the simultaneous shock magnetization and demagnetization of rocks, PEPI 182, 42-49,
664 doi:10.1016/j.pepi.2010.06.009.

665 Gattacceca, J., Boustie, M., Weiss, B.P., Rochette, P., Lima, E.A., Fong, L.E., Baudenbacher,
666 F.J., (2006). Investigating impact demagnetization through laser impacts and SQUID
667 microscopy, Geology 34, 333-336, doi:10.1130/G21898.1.

668 Gattacceca, J., Lamali, A., Rochette, P., Boustie, M., Berthe, L., (2007). The effects of
669 explosive-driven shocks on the natural remanent magnetization and the magnetic properties
670 of rocks, PEPI 162, 85-98, doi:10.1016/j.pepi.2007.1003.1006.

671 Gilder, S.A., Le Goff, M., (2008). Systematic pressure enhancement of titanomagnetite
672 magnetization, GRL 35, L10302, doi:10.1029/2008GL033325.

673 Gilder, S.A., Le Goff, M., Chervin, J.-C., (2006). Static stress demagnetization of single and
674 multi-domain magnetite with implications for meteorite impacts, High Pressure Research 26,
675 539-547, doi:510.1080/08957950601092085.

676 Gilder, S.A., LeGoff, M., Chervin, J.-C., Peyronneau, J., (2004). Magnetic properties of single
677 and multi-domain magnetite under pressures from 0 to 6 GPa, GRL 31,
678 doi:10.1029/2004GL019844.

679 Graham, J.W., Buddington, A.F., Balsley, J.R., (1957). Stress-induced magnetizations of some
680 rocks with analyzed magnetic minerals, JGR 62, 465-474, doi:10.1029/JZ062i003p00465.

681 Halekas, J.S., Lillis, R.J., Purucker, M.E., Louzada, K.L., Stewart, S.T., Manga, M., (2009).
682 Interpreting lunar impact demagnetization singatures using Lunar Prospector
683 Magnetometer/Electron Reflectometer data, LPSC XL Abs. No. 1354.

684 Hamano, Y., (1983). Experiments on the Stress Sensitivity of Natural Remanent Magnetization,
685 J. Geomagn. Geoelectr. 35, 155-172.

686 Hargraves, R.B., Perkins, W.E., (1969). Investigations of the Effect of Shock on Natural
687 Remanent Magnetization, JGR 74, 2576-2589, doi:10.1029/JB074i010p02576.

688 Harrison, C.G.A., (2000). Questions About Magnetic Lineations in the Ancient Crust of Mars,
689 Science 287, 547a, doi:10.1126/science.287.5453.547a.

690 Hood, L.L., Richmond, N.C., Harrison, K.P., Lillis, R.J., (2007). East-west trending magnetic
691 anomalies in the Southern Hemisphere of Mars: Modeling analysis and interpretation, Icarus
692 191, 113-131, doi:10.1016/j.icarus.2007.04.025.

693 Hood, L.L., Richmond, N.C., Pierazzo, E., Rochette, P., (2003). Distribution of crustal magnetic
694 fields on Mars: Shock effects of basin-forming impacts, GRL 30, 1281-1284,
695 doi:10.1029/2002GL016657.

696 Ivanov, A.B., Melosh, H.J., Pierazzo, E., Basin-forming impacts: Reconnaissance modeling, in:
697 R.L. Gibson, W.U. Reimold, (Eds), Large Meteorite Impacts and Planetary Evolution IV
698 Special Paper 465, Geological Society of America, 2010, pp. 29-49,
699 doi:10.1130/2010.2465(03).

700 Jackson, M., Borradaile, G., Hudleston, P., Banerjee, S., (1993). Experimental Deformation of
701 Synthetic Magnetite-Bearing Calcite Sandstones: Effects on Remanence, Bulk Magnetic
702 Properties, and Magnetic Anisotropy, JGR 98, 383-401, doi:10.1029/92JB01028.

703 Kinoshita, H., (1968). Studies on Piezo-Magnetization (III)-PRM and Relating Phenoma-, J.
704 Geomagn. Geoelectr. 20, 155-167.

705 Kirschvink, J.L., Maine, A.T., Vali, H., (1997). Paleomagnetic Evidence of a Low-Temperature
706 Origin of Carbonate in the Martian Meteorite ALH84001, Science 275, 1629-1633,
707 doi:10.1126/science.275.5306.1629.

708 Kletetschka, G., Connerney, J.E.P., Ness, N.F., Acuña, M.H., (2004). Pressure effects on martian
709 crustal magnetization near large impact basins, MAPS 39, 1839-1848, doi:10.1111/j.1945-
710 5100.2004.tb00079.x.

711 Klingelhöfer, G., Morris, R.V., Bernhardt, B., Schröder, C., Rodionov, D.S., de Souza, P.A., Jr,
712 Yen, A., Gellert, R., Evlanov, E.N., Zubkov, B., Foh, J., Bonnes, U., Kankeleit, E., Gütlich,
713 P., Ming, D.W., Renz, F., Wdowiak, T., Squyres, S.W., Arvidson, R.E., (2004). Jarosite and
714 Hematite at Meridiani Planum from Opportunity's Mössbauer Spectrometer, Science 306,
715 1740-1745, doi:10.1126/science.1104653.

716 Kohout, T., Deutsch, A., Pesonen, L.J., Hornemann, U., The magnetic behavior of synthetic
717 magnetite induced by shock recovery experiments in the range between 10 and 45 GPa,
718 Bridging the Gap II: Effect of Target Properties on the Impact Cratering Process, Saint-
719 Hubert, Canada, 2007, p. Abstract #8036.

720 Kontny, A., Elbra, T., Just, J., Pesonen, L.J., Schleicher, A.M., Zolk, J., (2007). Petrography and
721 shock-related remagnetization of pyrrhotite in drill cores from the Bosumtwi Impact Crater
722 Drilling Project, Ghana, MAPS 42, 811-827, doi:10.1111/j.1945-5100.2007.tb01077.x.

723 Langel, R.A., Phillips, J.D., Horner, R.J., (1982). Initial scalar magnetic anomaly map from
724 MAGSAT, GRL 9, 269-272, doi:10.1029/GL009i004p00269.

725 Lillis, R.J., Frey, H.V., Manga, M., (2008). Rapid decrease in Martian crustal magnetization in
726 the Noachian era: Implications for the dynamo and climate of early Mars, GRL 35, L14203,
727 doi:10.1029/2008GL034338.

728 Lillis, R.J., Frey, H.V., Manga, M., Mitchell, D.L., Lin, R.P., Acuña, M.H., Bougher, S.W.,
729 (2008). An improved crustal magnetic field map of Mars from electron reflectometry:
730 Highland volcano magmatic history and the end of the martian dynamo, Icarus 194, 575-596,
731 doi:10.1016/j.icarus.2007.09.032.

Lillis, R.J., Purucker, M.E., Halekas, J.S., Louzada, K.L., Stewart-Mukhopadhyay, S.T., Manga, M., Frey, H.V., (2010). Study of impact demagnetization at Mars using Monte Carlo modeling and multiple altitude data, JGR 115, E07007, doi:10.1029/2009JE003556.

Longhi, J., Knittle, E., Holloway, J.R., Wänke, H., 6. The bulk composition, mineralogy and internal structure of Mars, in: H.H. Kieffer, B.M. Jakosky, C.W. Snyder, M.S. Matthews, (Eds), Mars, Space Science, The University of Arizona Press, Tuscon, 1992, pp. 184-208,

Lorand, J.-P., Chevrier, V., Sautter, V., (2005). Sulfide mineralogy and redox conditions in some shergottites, MAPS 40, 1257–1272, doi:10.1111/j.1945-5100.2005.tb00187.x.

Louzada, K.L., Stewart, S.T., (2009). Effects of Planet Curvature and Crust on the Shock Pressure Field around Impact Basins, GRL 36, L15203, doi:10.1029/2009GL037869.

Louzada, K.L., Stewart, S.T., Weiss, B.P., (2007). Effect of shock on the magnetic properties of pyrrhotite, the Martian crust, and meteorites, GRL 34, L05204, doi:10.1029/2006GL027685.

Louzada, K.L., Stewart, S.T., Weiss, B.P., Gattacceca, J., Bezaeva, N.S., (2010). Shock and static pressure demagnetization of pyrrhotite and implications for the Martian crust, EPSL 290, 90–101, doi:10.1016/j.epsl.2009.12.006.

Louzada, K.L., Weiss, B.P., Maloof, A.C., Stewart, S.T., Swanson-Hysell, N.L., Soule, S.A., (2008). Paleomagnetism of Lonar impact crater, India, EPSL 275, 308-319, doi:10.1016/j.epsl.2008.08.025.

Madsen, M.B., Goetz, W., Bertelsen, P., Binau, C.S., Folkmann, F., Gunnlaugsson, H.P., ı´ Hjøllum, J., Jensen, J., Kinch, K.M., Leer, K., Madsen, D.E., Merrison, J., Olsen, M., Arneson, M.H., Bell III, J.F., Gellert, R., Herkenhoff, K.E., Johnson, J.R., Johnson, M.J., Klingelhöfer, G., McCartney, E., Ming, D.W., Morris, R.V., Proton, J.B., Rodionov, D., Sims, M., Squyres, S.W., Wdowiak, T., Yen, A.S., (2009). Overview of the magnetic properties experiments on the Mars Exploration Rovers, JGR 114, E06S90, doi:10.1029/2008JE003098.

Martelli, G., Newton, G., (1977). Hypervelocity cratering and impact magnetisation of basalt, Nature 269, 478-480, doi:10.1038/269478a0.

Martin, R.J., III, Noel, J.S., (1988). The influence of stress path on thermoremanent magnetization, GRL 15, 507-510, doi:10.1029/GL015i005p00507.

McEnroe, S.A., Skilbrei, J.R., Robinson, P., Heidelbach, F., Langenhorst, F., Brown, L.L., (2004). Magnetic anomalies, layered intrusions and Mars, GRL 31, L19601, doi:10.1029/2004GL020640.

McSween Jr, H.Y., Treiman, A.H., Chapter 6: Martian meteorites, in: J.J. Papike, (Ed), Planetary Materials, Reviews in Mineralogy 36, 1998, p. 53,

Melosh, H.J., (1984). Impact Ejection, Spallation, and the Origin of Meteorites, Icarus 59, 234-260, doi:10.1016/0019-1035(84)90026-5.

768 Melosh, H.J., Impact Cratering: A Geologic Process, Oxford University Press, New York, 1989,
769 245 pp.

770 Mohit, P.S., Arkani-Hamed, J., (2004). Impact demagnetization of the martian crust, Icarus 168,
771 305-317, doi:10.1016/j.icarus.2003.12.005.

772 Nagata, T., (1966). Main Characteristics of Piezo-Magnetization and Their Qualitative
773 Interpretation, J. Geomagn. Geoelectr. 18, 81-97.

774 Nagata, T., (1970). Basic Magnetic Properties of Rocks Under the Effects of Mechanical
775 Stresses, Tectonophysics 9, 167-195, doi:10.1016/0040-1951(70)90015-6.

776 Nagata, T., (1971). Introductory Notes on Shock Remanent Magnetization and Shock
777 Demagnetization of Igneous Rocks, Pure and Appl. Geophys. 89, 159-177,
778 doi:10.1007/BF00875213.

779 Nagata, T., Carleton, B.J., (1969). Notes on Piezo-remanent Magnetization of Igneous Rocks II,
780 J. Geomagn. Geoelectr. 21, 427-445.

781 Nimmo, F., Gilmore, M.S., (2001). Constraints on the depth of magnetized crust on Mars from
782 impact craters, JGR 106, 12315-12323, doi:10.1029/2000JE001325.

783 Nimmo, F., Tanaka, K., (2005). Early Crustal Evolution on Mars, Annual Reviews Earth and
784 Planetary Science 33, 133-161, doi:10.1146/annurev.earth.33.092203.122637.

785 Ohnaka, M., Kinoshita, H., (1968). Effects of Uniaxial Compression on Remanent
786 Magnetization, J. Geomagn. Geoelectr. 20, 93-99.

787 Pearce, G.W., Karson, J.A., (1981). On Pressure Demagnetization, GRL 8, 725-728,
788 doi:10.1029/GL008i007p00725.

789 Pesonen, L.J., Deutsch, A., Hornemann, U., Langenhorst, F., (1997). Magnetic properties of
790 diabase samples shocked experimentally in the 4.5 to 35 GPa range, LPSC XXVIII 1087-
791 1088.

792 Pierazzo, E., Vickery, A.M., Melosh, H.J., (1997). A Reevaluation of Impact Melt Production,
793 Icarus 127, 408-423, doi:10.1006/icar.1997.5713.

794 Pohl, J., Bleil, U., Hornemann, U., (1975). Shock Magnetization and Demagnetization of Basalt
795 by Transient Stress up to 10 kbar, Journal of Geophysics 41, 23-41.

796 Rochette, P., Fillion, G., Ballou, R., Brunet, F., Ouladdiaf, B., Hood, L., (2003). High pressure
797 magnetic transition in pyrrhotite and impact demagnetization on Mars, GRL 30,
798 doi:10.1029/2003GL017359.

799 Rochette, P., Gattacceca, J., Chevrier, V., Hoffmann, V., Lorand, J.-P., Funaki, M., Hochleitner,
800 R., (2005). Matching Martian crustal magnetization and magnetic properties of Martian
801 meteorites, MAPS 40, 529-540, doi:10.1111/j.1945-5100.2005.tb00961.x.

802 Rochette, P., Lorand, J.-P., Fillion, G., Sautter, V., (2001). Pyrrhotite and the remanent
803 magnetization of SNC meteorites: a changing perspective of Martian magnetism, EPSL 190,
804 1-12, doi:10.1016/S0012-821X(01)00373-9.

805 Schultz, R.A., Frey, H.V., (1990). A New Survey of Multiring Impact Basins on Mars, JGR 95,
806 14175-14189, doi:10.1029/JB095iB09p14175.

807 Scott, E.R.D., Fuller, M., (2004). A possible source for the Martian crustal magnetic field, EPSL
808 220, 83-90, doi:10.1016/S0012-821X(04)00032-9.

809 Sekine, T., Kobayashi, T., Nishio, M., Takahashi, E., (2008). Shock equation of state of basalt,
810 Earth Planets and Space 60, 999-1003.

811 Shahnas, H., Arkani-Hamed, J., (2007). Viscous and impact demagnetization of Martian crust,
812 JGR 112, doi:10.1029/2005JE002424.

813 Shapiro, V.A., Ivanov, N.A., (1967). Dynamic Remanence and the Effect of Shock on the
814 Remanence of Strongly Magnetic Rocks, Doklady Akad. Nauk SSR - Geophysics 173, 6-8.

815 Smith, D.E., Zuber, M.T., Solomon, S.C., Phillips, R.J., Head, J.W., Garvin, J.B., Banerdt, W.B.,
816 Muhleman, D.O., Pettengill, G.H., Neumann, G.A., Lemoine, F.G., Abshire, J.B.,
817 Aharonson, O., Brown, C.D., Hauck, S.A., Ivanov, A.B., McGovern, P.J., Zwally, H.J.,
818 Duxbury, T.C., (1999). The Global Topography of Mars and Implications for Surface
819 Evolution, Science 284, 1495-1503, doi:10.1126/science.284.5419.1495.

820 Spudis, P.D., The geology of multi-ring impact basins: the Moon and other planets, Cambridge
821 University Press, Cambridge, 1993, 263 pp.

822 Srnka, L.J., Martelli, G., Newton, G., Cisowski, S.M., Fuller, M.D., Schaal, R.B., (1979).
823 Magnetic Field and Shock Effects and Remanent Magnetization in a Hypervelocity
824 Experiment, EPSL 42, 127-137, doi:10.1016/0012-821X(79)90198-5.

825 Stanley, S., Elkins-Tanton, L., Zuber, M.T., Parmentier, E.M., (2008). Mars' paleomagnetic field
826 as the result of a single-hemisphere dynamo, Science 321, 1822-1825,
827 doi:10.1126/science.1161119.

828 Stott, P.M., Stacey, F.D., (1960). Magnetostriction and Palaeomagnetism of Igneous Rocks, JGR
829 65, 2419-2424, doi:10.1029/JZ065i008p02419.

830 Tanaka, K.L., Leonard, G.J., (1995). Geology and landscape evolution of the Hellas region of
831 Mars, JGR 100, 5407-5432, doi:10.1029/94JE02804.

832 Voorhies, C.V., (2008). Thickness of the magnetic crust of Mars, JGR 113, E04004, doi:
833 10.1029/2007JE002928.

834 Voorhies, C.V., Sabaka, T.J., Purucker, M., (2002). On magnetic spectra of Earth and Mars, JGR
835 107, doi:10.1029/2001JE001534.

836 Wasilewski, P., (1976). Shock-loading meteoritic b.c.c. metal above the pressure transition:
837 remanent-magnetization stability and microstructure, PEPI 11, P5-P11, doi:10.1016/0031-
838 9201(76)90060-1.

839 Watters, W.A., Zuber, M.T., Hager, B.H., (2009). Thermal perturbations caused by large impacts
840 and consequenses for mantle convection, JGR 114, E02001, doi:10.1029/2007JE002964.

841 Weiss, B.P., Fong, L.E., Vali, H., Lima, E.A., Baudenbacher, F.J., (2008). Paleointensity of the
842 ancient Martian magnetic field, GRL 35, L23207, doi:10.1029/2008GL035585.

843 Weiss, B.P., Kirschvink, J.L., Baudenbacher, F.J., Vali, H., Peters, N.T., Macdonald, F.A.,
844 Wikswo, J.P., (2000). A Low Temperature Transfer of ALH84001 from Mars to Earth,
845 Science 290, 791-795, doi:10.1126/science.290.5492.791.

846 Weiss, B.P., Pedersen, S., Garrick-Bethell, I., Stewart, S.T., Louzada, K.L., Maloof, A.C.,
847 Swanson-Hysell, N.L., (2010). Paleomagnetism of impact spherules from Lonar crater, India
848 as a test for impact-generated fields, EPSL doi:10.1016/j.epsl.2010.07.028.

849 Weiss, B.P., Shuster, D.L., Stewart, S.T., (2002). Temperatures on Mars from $^{40}Ar/^{39}Ar$
850 thermochronology of ALH84001, EPSL 201, 465-472, doi:10.1016/S0012-821X(02)00729-
851 X.

852 Weiss, B.P., Vali, H., Baudenbacher, F.J., Kirschvink, J.L., Stewart, S.T., Shuster, D.L., (2002).
853 Records of an ancient Martian magnetic field in ALH84001, EPSL 201, 449-463,
854 doi:10.1016/S0012-821X(02)00728-8.
855
856
857

858 **Figure Captions**

859 **Figure 1.** Spherical projection maps of Mars' crustal magnetic field magnitude, centered on
860 45° S, 12° E, from a) electron reflectometer measurements at 185 km altitude and b)
861 magnetometer measurements at 400 km altitude from the Mars Global Surveyor (Lillis, et al.,
862 2008; Lillis, et al., 2010). The large demagnetized basins Hellas (He), Argyre (Ag) and
863 Prometheus (Pr) are labeled. The other circles represent older, magnetized basins identified by
864 Frey (2008).

865 **Figure 2.** A schematic of the different crustal magnetic modification processes applicable to
866 the formation of a (simple) crater in the absence of an ambient magnetic field. After Melosh
867 (1989) and numerical simulations of Lonar crater, India (Figure 3 in Louzada, et al., 2008). Color
868 online, grayscale in print.

869 **Figure 3.** Schematic representation of conventional shock pressure contours (P_1-P_6) and their
870 relationship to spacecraft magnetometry for a large impact onto a flat planet. The shock pressure
871 decays with distance from the impact point. Near the surface, shock waves interfere with
872 rarefaction waves from the free-surface, effectively reducing the shock pressure. The depth of
873 the interference zone depends on the size of the impactor and the curvature of the planet; for
874 large impacts the interference zone is deep and encompasses the entire (magnetic) crust. Pressure
875 decay at depths below the interference zone is hemispherical. Spacecraft magnetic measurements
876 above impact basins show decreased (nearly zero) intensities of the crustal magnetic field at
877 altitude. No vertical exaggeration.

878 **Figure 4.** Shock pressure contour results from hydrocode simulations of 125 km and (black
879 lines) and 230 km (grey lines) radius impactors on Mars at 9 km/s (Louzada and Stewart, 2009).

Because Hellas is an elliptical basin, ranges for its inner and outer topographic boundaries are given, rather than single values, and were determined from Mars Orbital Laser Altimeter (MOLA) topography data (Smith, et al., 1999).

Figure 5. Demagnetization as a function of pressure over Hellas Basin: azimuthally averaged shock pressure contours in the magnetic portion of the crust plotted over the averaged magnetic field intensity at altitude. The solid and dashed lines illustrate the shock pressure contours (100 km radial bins, averaged over the crust between 10 and 50 km depth) resulting from the hydrocode simulations of impacts by125-km and 230-km radius projectiles at 9 km/s (1σ error bars), respectively. Azimuthally averaged crustal magnetic field intensity at 185 km altitude (with 100 km smoothing; Lillis, et al., 2008) over Hellas basin between azimuths of 300° and 120° with respect to geographic N (clockwise) increases with distance. The dark grey shaded region represents 1σ error bars. The sensitivity threshold for detecting unambiguously crustal fields is 4 nT (horizontal dash-dotted line).

Figure 6. Schematic of the stress duration and strain rate regimes for different experimental techniques and planetary-scale impact cratering (Bezaeva, et al., 2010; Borradaile and Mothershill, 1991; Boustie and Cottet, 1991; Melosh, 1989; Rochette, et al., 2003).

Figure 7. Compilation of selected static (hydrostatic - open symbols) and dynamic (drop, plate impact, laser shock and explosive shock - solid symbols) pressure experiments (below 5 GPa) on magnetite (A), titanomagnetite (B), hematite (C), titanohematite (D), and pyrrhotite (E). Red, green, orange, and blue symbol colors indicate single-domain* (SD)/superparamagnetic* (SP), single-domain/pseudo-single-domain* (PSD), pseudo-single-domain/multidomain* (MD), and multidomain samples, respectively. For more information and sources see Table 1.

***Research Highlights**

- Compiling the available pressure demagnetization data indicates a universal trend.
- All minerals demagnetize substantially as a result of compression below 5 GPa.
- Experimental demagnetization data do not lend mineral specific thumbprints.
- At present, we cannot constrain the mineralogy on Mars from demagnetized basins.

Figure 1 color

Click here to download Figure: Figure 1 revised color.pdf

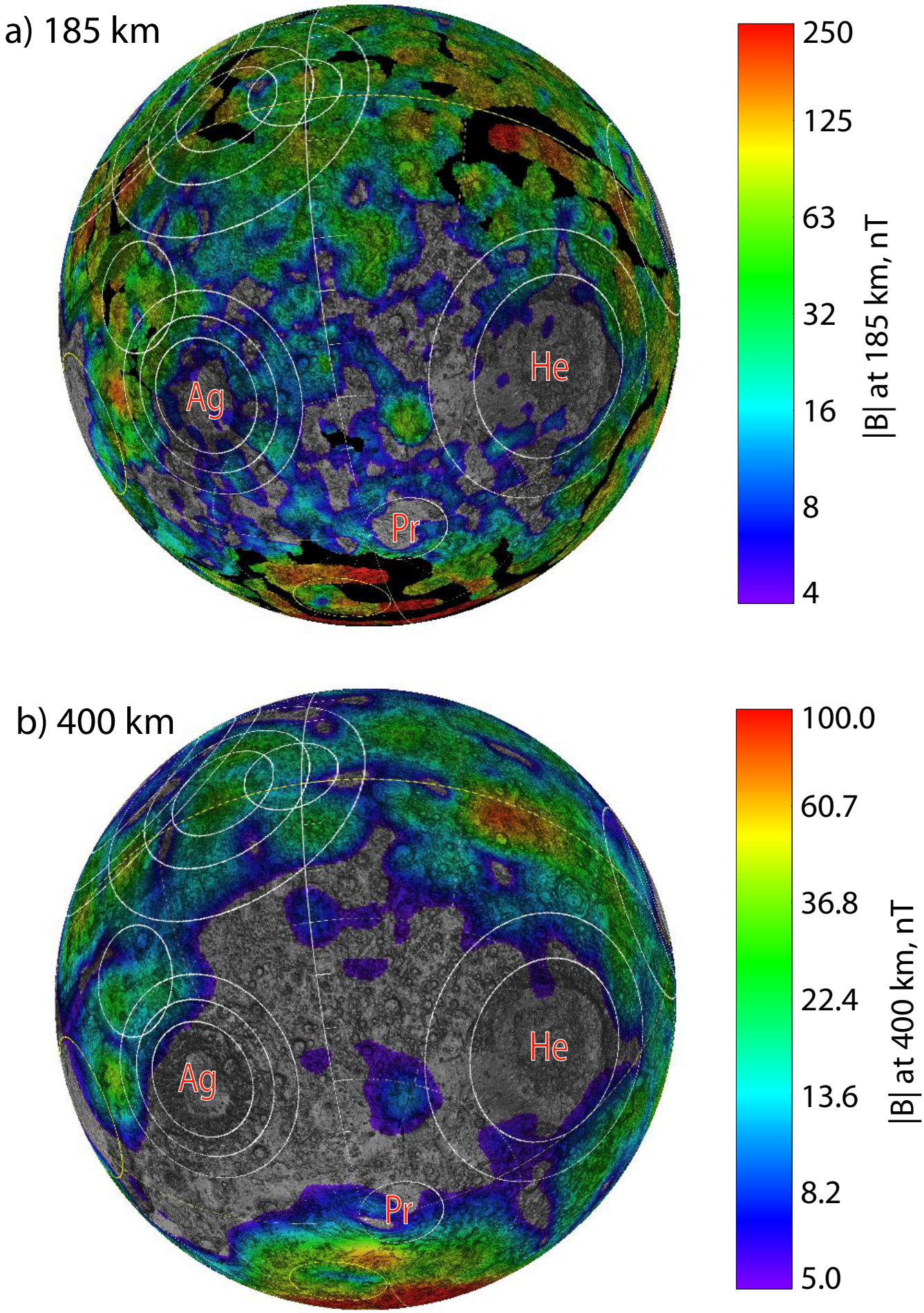

Figure 2 b&w

Click here to download Figure: Figure 2 revised B&W v2.eps

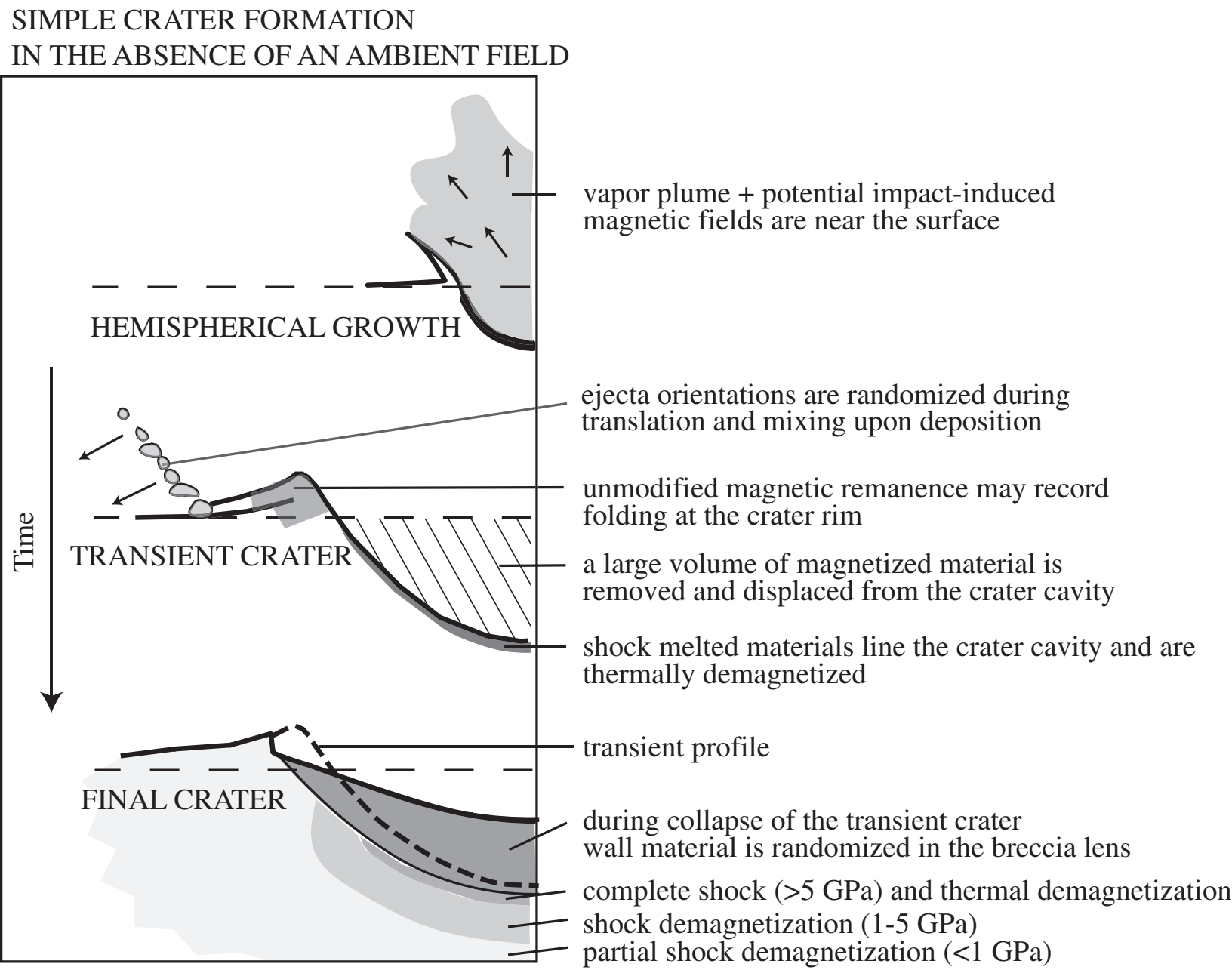

Figure 2 color

Click here to download Figure: Figure 2 revised color v2.eps

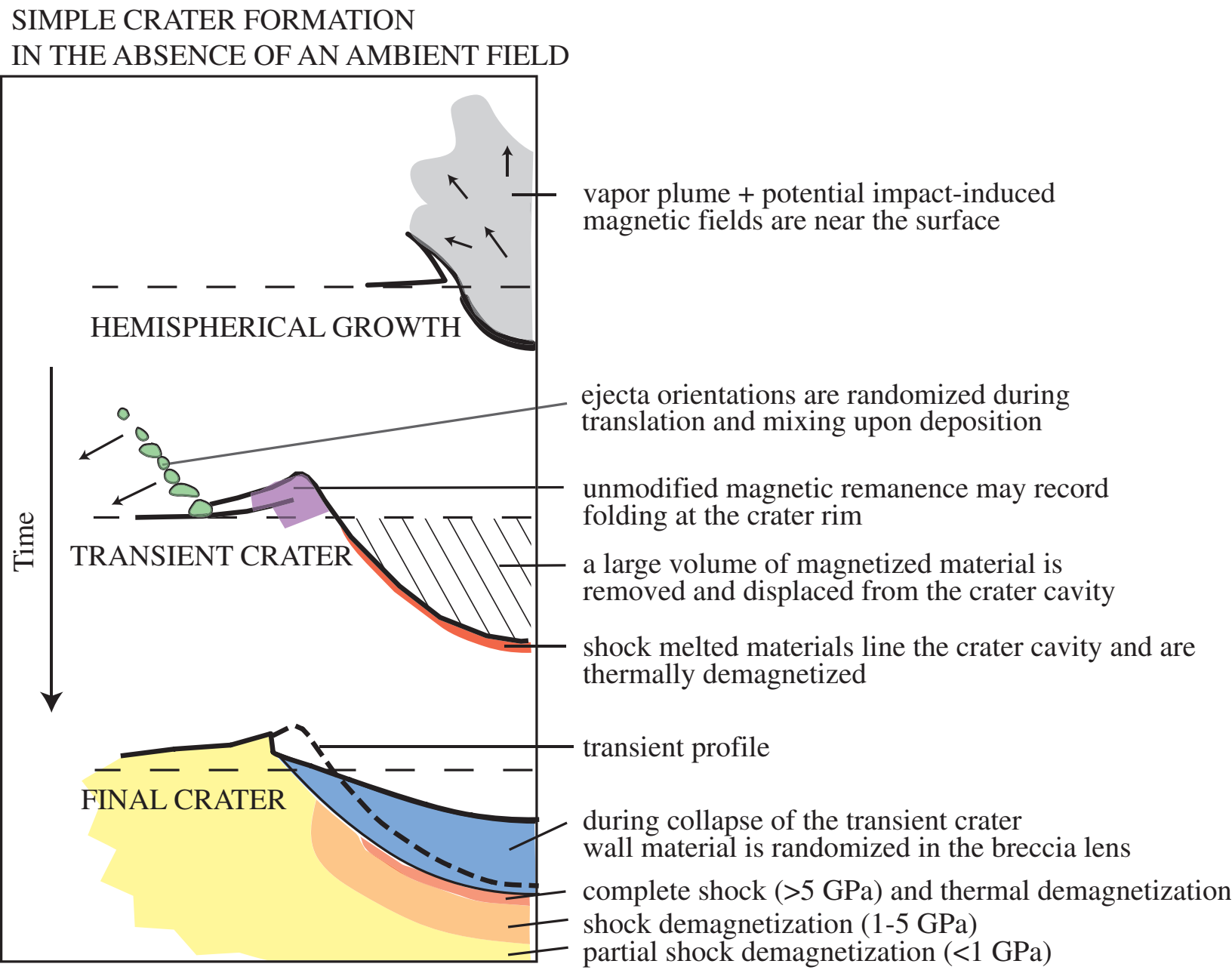

Figure 3 b&w

Click here to download Figure: Figure 3 revised B&W.eps

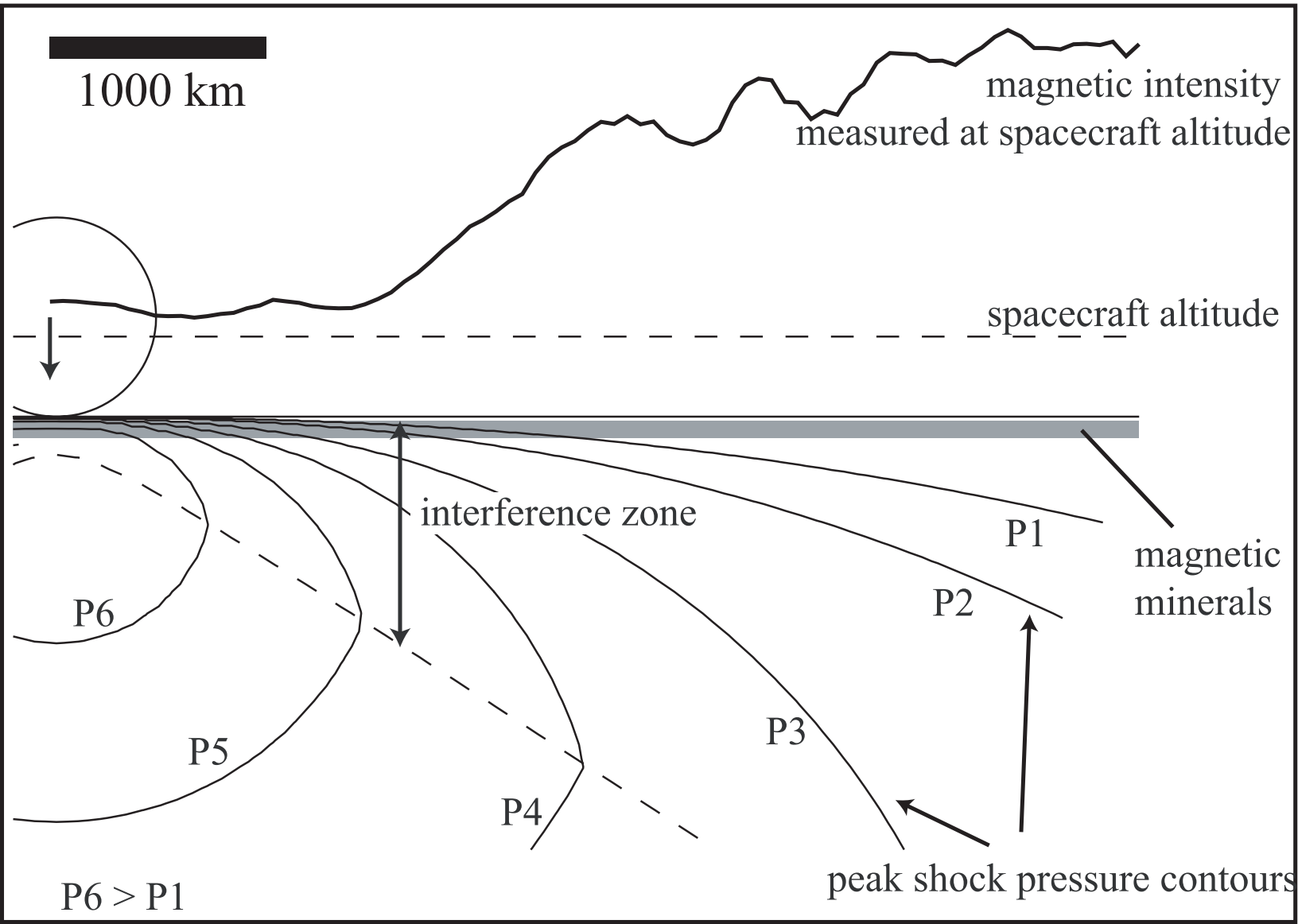

Figure 4 b&w

Click here to download Figure: Figure 4 revised B&W.eps

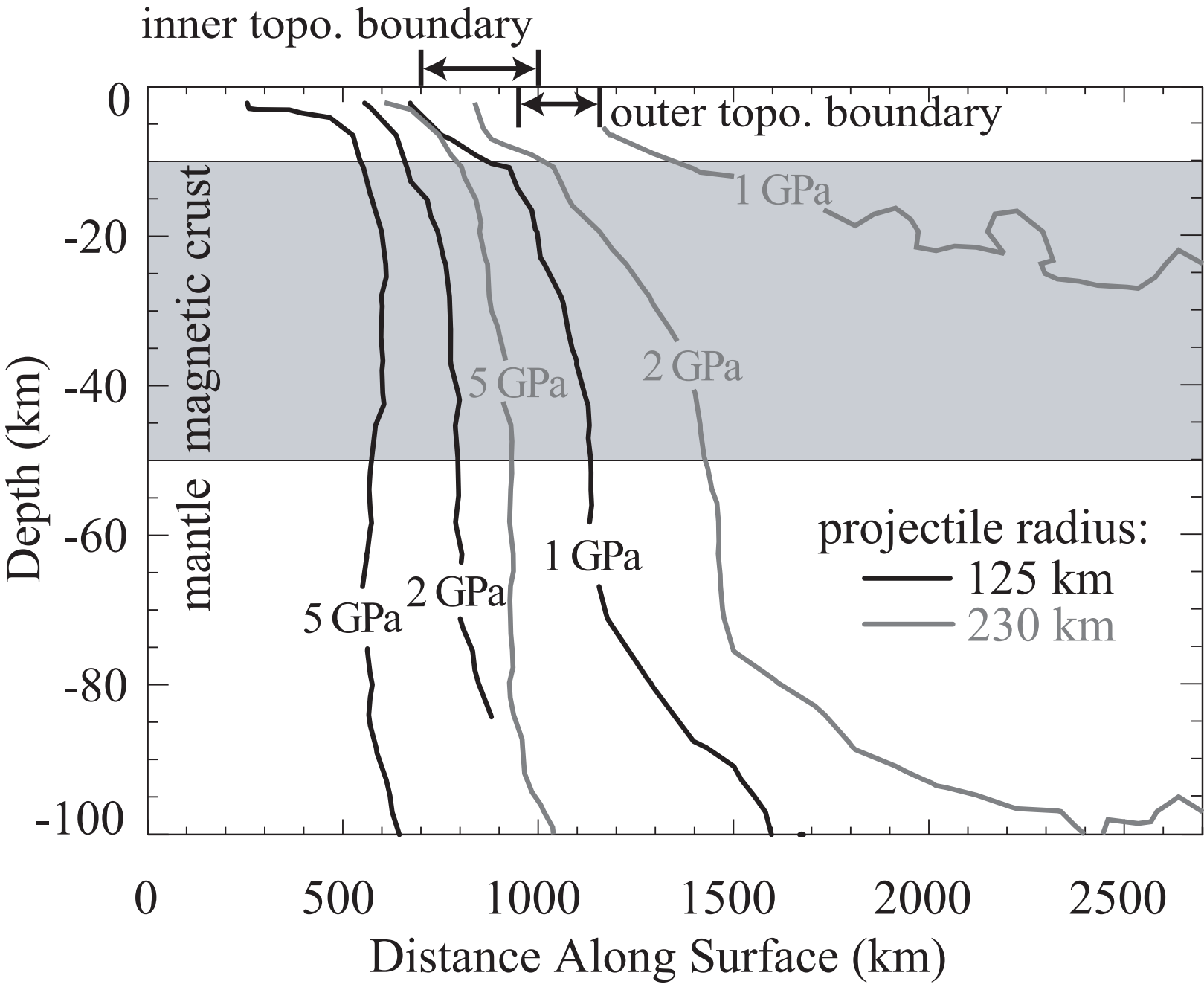

Figure 5 b&w

Click here to download Figure: Figure 5 revised B&W v2.eps

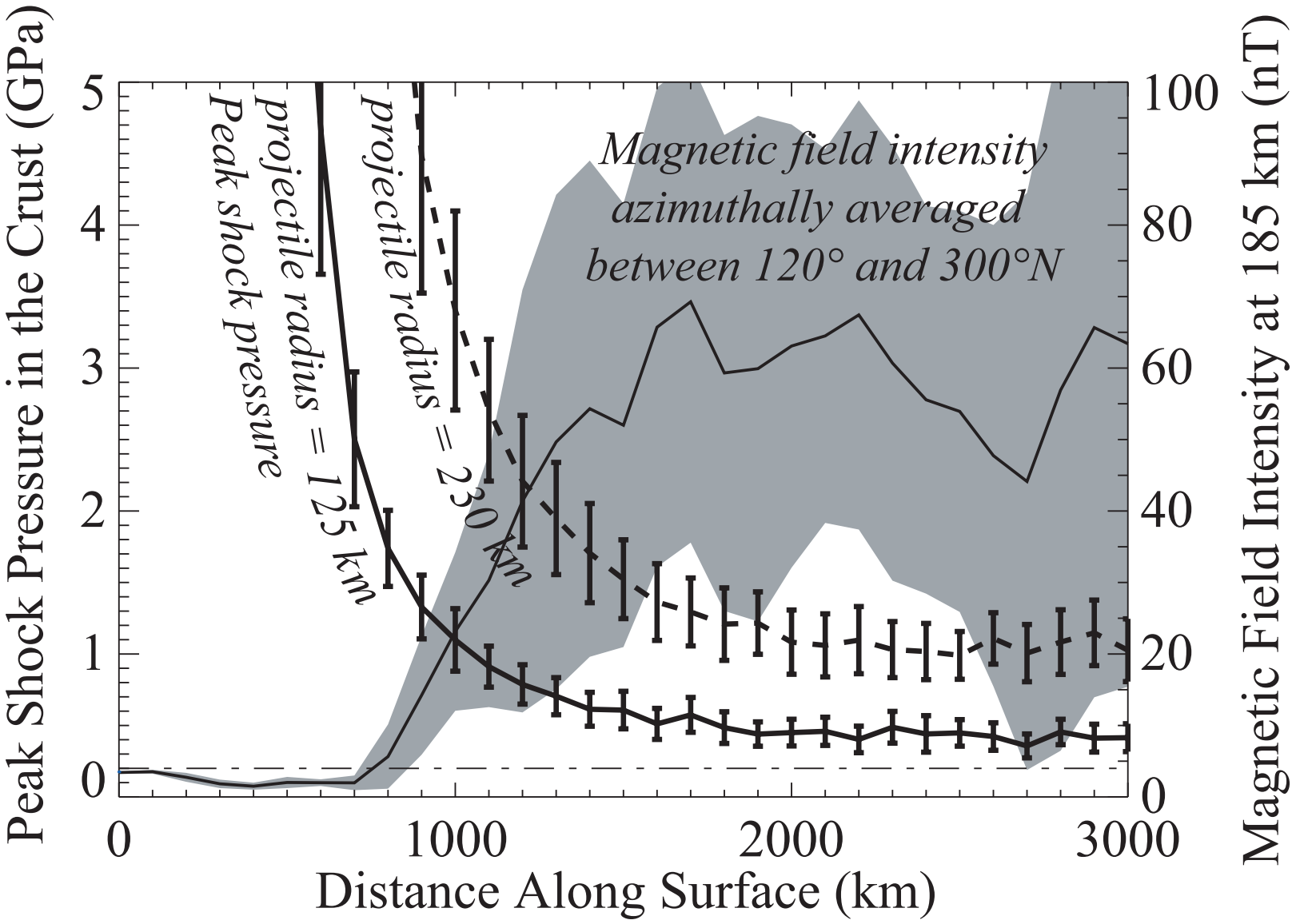

Figure 6 b&w

Click here to download Figure: Figure 6 revised B&W.eps

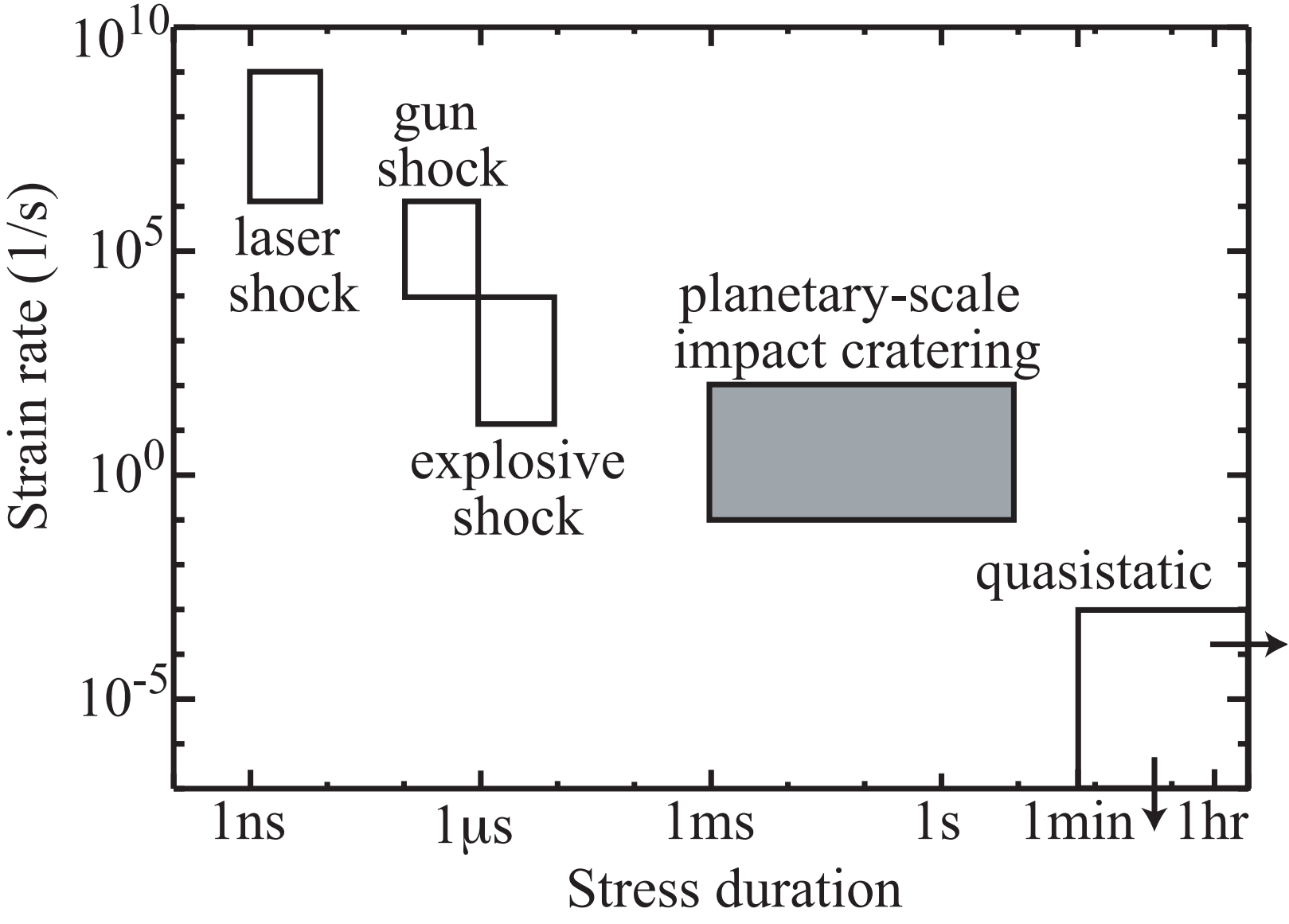

Figure 7 color

Click here to download Figure: Figure 7 revised color v2.eps

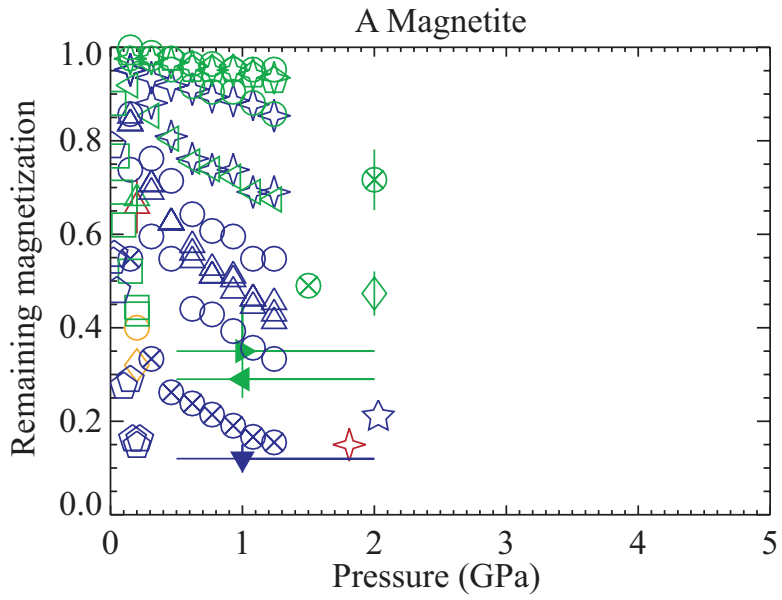

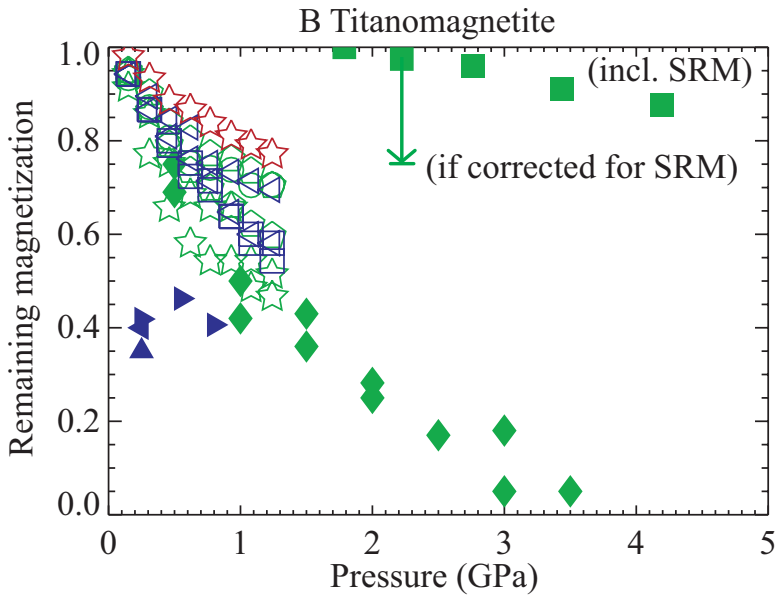

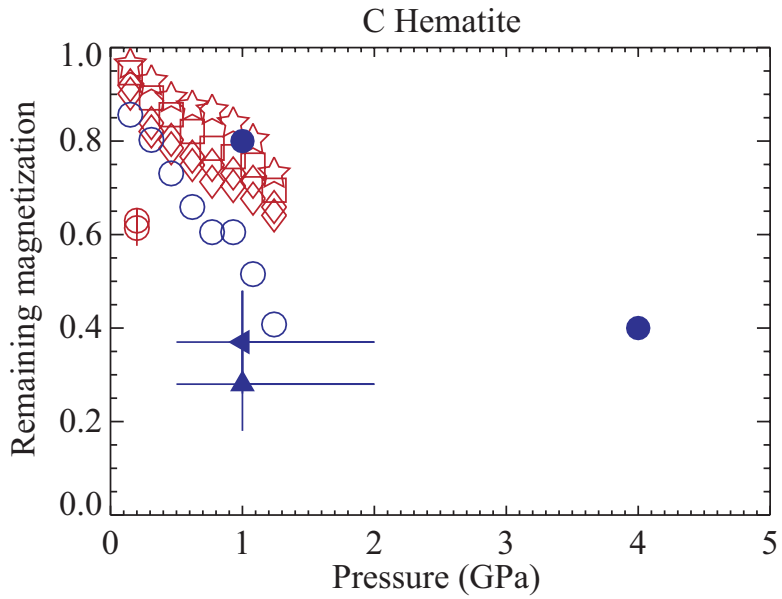

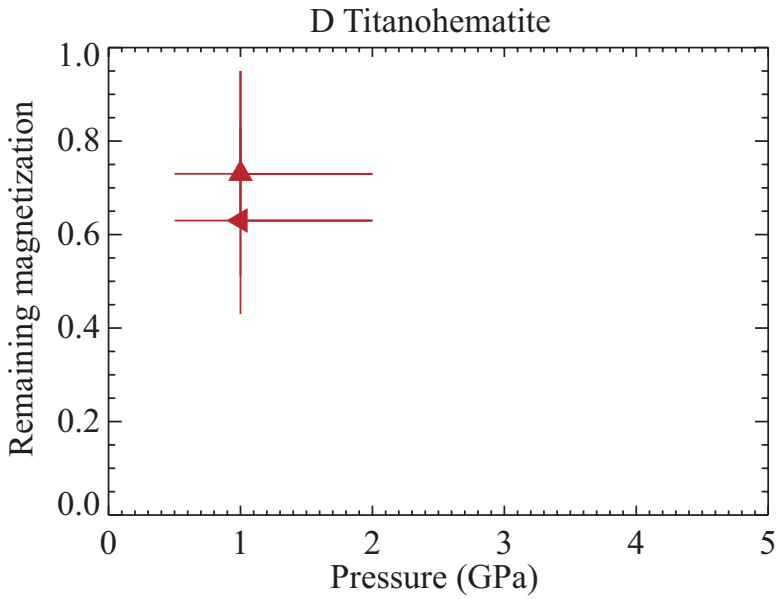

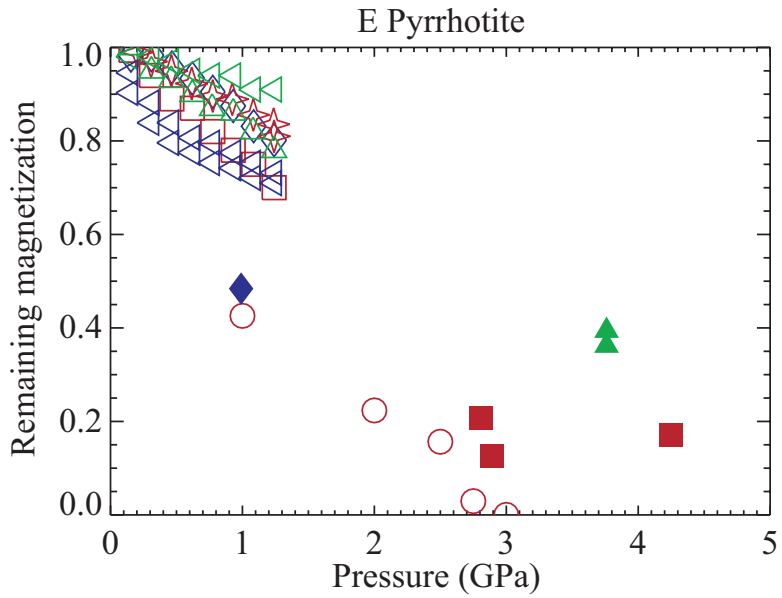

Red = Single-domain,
Single-domain/Superparamagnetic
Green = Pseudo-single-domain,
Single-domain/Pseudo-single-domain
Orange = Pseudo-single-domain/Multidomain
Blue = Multidomain
Solid symbols = high strain rate
Open symbols = low strain rate
*Shock direction parallel to [00l]
See Table 1 for more information and references.

text box
Click here to download Figure: Text Box.pdf

Glossary of magnetic terms:

Blocking temperature = the temperature at which a ferromagnetic material can be regarded as being superparamagnetic (on a geological timescale).

Coercivity = the intensity of the applied magnetic field required to reduce the magnetization (induced + remanent) of a material to zero after magnetic saturation.

Coercivity of remanence = the intensity of the applied field required to reduce the remanence of a material to zero after magnetic saturation.

Curie temperature = the temperature at which the long-range ordering of atomic moments disappears because of local thermal fluctuations.

Domain = a region within a magnetic grain of constant magnetization. Because the magnetization between domains is of opposite sign, the net magnetization of the grain is smaller than the saturation magnetization. Domain walls separating domains are of a finite width and can move when exposed to an applied field resulting in a change in net magnetization.

Multidomain = grains with one or more domain. Because domain walls can move inside the grain, multidomain grains have a lower coercivity than single-domain grains.

Paramagnetism = a condition that allows materials with non-interacting atomic moments to retain a small induced magnetization parallel to the ambient field. The material cannot retain a remanence after the field is removed.

Pseudo-single domain = a multidomain domain grain with similar magnetic properties as single-domain grains.

Remanent magnetization (magnetic remanence) = the magnetization of a material measured in a zero field (no induced magnetization is present).

Single-domain = single-domain grains have only one domain. Because they must change their magnetization by rotation, single-domain grains generally have a higher coercivity than multidomain grains.

Spontaneous magnetization = a property of ferromagnetic materials that, unlike paramagnetic materials, retain a remanent magnetization after removal of a magnetizing field due to the alignment of atomic moments.

Superparamagnetism = a thermally activated condition that allows for the spontaneous reversal of magnetic moment in very small single-domain grains to be rapid enough that it cannot stably retain a remanence.

Table
Click here to download Table: Table 1.doc

Table 1. Pressure demagnetization experiments of selected rocks and minerals. (Summarized in Figure 7.)

Domain size	*Sample Description*	*Experiment type*	*Remanence type*	*Pressure range* (GPa)	*Figure & Symbol*	*Comments*	*Source*
	Magnetite (Ti<40%)				(Figure 7A)		
SD	Pure magnetite	hydrostatic	IRM	0.16-1.81			(Gilder, et al., 2006)
SD	Ancaster limestone	hydrostatic	IRM	0.2			(Borradaile, 1992)
SD/PSD	Magnetite dispersed naturally in green spinel	drop	SIRM	~1 (-0.5/+1)			(Kletetschka, et al., 2004)
SD/PSD	Magnetite dispersed naturally in green spinel	drop	NRM	~1 (-0.5/+1)			(Kletetschka, et al., 2004)
PSD	Ancaster limestone	hydrostatic	SIRM	0.2			(Borradaile, 1993)
PSD	Synthetic (unspecified)	hydrostatic	SIRM, NRM (unspecified)	2			(Pearce and Karson, 1981)
PSD	Rock samples (unspecified)	hydrostatic	SIRM, NRM (unspecified)	2			(Pearce and Karson, 1981)
PSD	Martian Nakhlite NWA998	hydrostatic	SIRM	0-1.24		under pressure	(Bezaeva, et al., 2007)
PSD	Chemically precipitated magnetite and calcite rock analogue	hydrostatic	two-component IRM	0.025-0.200			(Borradaile and Jackson, 1993)
PSD?	Ignimbrite	hydrostatic	SIRM	0-1.24		under pressure	(Bezaeva, et al., 2010)
PSD?	Andesite	hydrostatic	SIRM	0-1.24		under pressure	(Bezaeva, et al., 2010)
PSD?	Granite	hydrostatic	SIRM	0-1.24		under pressure	(Bezaeva, et al., 2010)
PSD/MD	Calcite magnetite aggregate	hydrostatic	ARM	0.2			(Borradaile, 1993)
PSD/MD	Calcite magnetite aggregate	hydrostatic	SIRM	0.2			(Borradaile, 1993)
MD	Granite	hydrostatic	SIRM	0-1.24		under pressure	(Bezaeva, et al., 2010)
MD?	Ignimbrite	hydrostatic	SIRM	0-1.24		under pressure	(Bezaeva, et al., 2010)
MD	Pure magnetite	hydrostatic	IRM	0-2.03			(Gilder, et al., 2006)
MD	Natural crushed magnetite with calcite	hydrostatic	2-component IRM	0.010-0.220			(Borradaile and Jackson, 1993)
MD?	Microdiorite	hydrostatic	SIRM	0-1.24		under pressure	(Bezaeva, et al., 2010)
MD?	Synthetic	hydrostatic	SIRM	0-1.24		under pressure	(Bezaeva, et al., 2010)
MD	Pure magnetite	drop	NRM	~1 (-0.5/+1)			(Kletetschka, et al., 2004)

	Titanomagnetite (Ti>40t%)				(Figure 7B)		
SD	Martian shergottite Los Angeles	hydrostatic	SIRM	0-1.24		under pressure	(Bezaeva, et al., 2007)
PSD	Basalt	hydrostatic	SIRM	0-1.24		under pressure	(Bezaeva, et al., 2007); (Bezaeva, et al., 2010)
MD	Basalt, Lonar	hydrostatic	SIRM	0-1.24		under pressure	(Bezaeva, et al., 2010)
MD	Basalt, Lonar	hydrostatic	ARM	0-1.24		under pressure	(Bezaeva, et al., 2010)
PSD	Basalt, $Fe_{0.25}Ti_{0.75}O_4$	explosive shock	NRM	2.9-31.3		demagnetization +SRM acquisition	(Gattacceca, et al., 2007)
PSD	Basalt, $[Fe_3O_4]_{0.54}[Fe_2TiO_4]_{0.46}$	laser shock	SIRM	0-3.5		shifted up 20% to compensate for offset due to sensor to surface distance between pre and postshock measurements	(Gattacceca, et al., 2006)
MD	Ignimbrite	hydrostatic	SIRM	0-1.24		under pressure	(Bezaeva, et al., 2007)
MD?	Andesite	hydrostatic	SIRM	0-1.24		under pressure	(Bezaeva, et al., 2007)
MD/SD	Basalt, $[Fe_3O_4]_{0.46}[Fe_2TiO_4]_{0.54}$	shock	SIRM	0.25			(Pohl, et al., 1975)
MD/SD	Basalt, $[Fe_3O_4]_{0.46}[Fe_2TiO_4]_{0.54}$	shock	TRM	0.25			(Pohl, et al., 1975)
MD/SD	Basalt, $[Fe_3O_4]_{0.46}[Fe_2TiO_4]_{0.54}$	shock	NRM	0.25, 0.55, 0.8			(Pohl, et al., 1975)
	Hematite				(Figure 7C)		
SD	Rhyolite	hydrostatic	SIRM	0-1.24		under pressure	(Bezaeva, et al., 2010)
SD	Synthetic aggregates with calcite and Portland cement with hematite (<0.5μm) pigment	hydrostatic	near SIRM	0.2			(Borradaile, 1993) (Borradaile, 1992)
SD?	Radiolarite	hydrostatic	SIRM	0-1.24		under pressure	(Bezaeva, et al., 2010)
SD?	Jasper	hydrostatic	SIRM	0-1.24		under pressure	(Bezaeva, et al., 2010)
MD	Synthetic	hydrostatic	SIRM	0-1.24		under pressure	(Bezaeva, et al., 2010)
MD	Pure hematite	drop	NRM	~1 (-0.5/+1)			(Kletetschka, et al., 2004)
MD	Pure hematite	drop	SIRM	~1 (-0.5/+1)			(Kletetschka, et al., 2004)
MD	Granite	gun shock	NRM	1-4			(Cisowski, et al., 1976)

	Titanohematite				(Figure 7D)		
SD	Exsolved ($Fe_{2-x}Ti_xO_3$, x<0.2)	drop	NRM	~1 (-0.5/+1)	▲		(Kletetschka, et al., 2004)
SD	Exsolved ($Fe_{2-x}Ti_xO_3$, x<0.2)	drop	SIRM	~1 (-0.5/+1)	◀		(Kletetschka, et al., 2004)
	Pyrrhotite				(Figure 7E)		
SD/SP	Pure, nodule	hydrostatic	SIRM	1.74-5.67	□	under pressure	(Bezaeva, et al., 2010; Louzada, et al., 2007, 2010)
SD/SP	Pure, nodule	plate impact	near SIRM	1.74-5.67	■		(Louzada, et al., 2007, 2010)
SD	Pure, Ducktown	hydrostatic	SIRM	1-3	○		(Rochette, et al., 2003)
SD	Basaltic shergottite NWA 1068	hydrostatic	SIRM	0-1.24	✧	under pressure	(Bezaeva, et al., 2007)
PSD	Rumuruti chondrite NWA 753	hydrostatic	SIRM	0-1.24	◁	under pressure	(Bezaeva, et al., 2010)
PSD	Schist	hydrostatic	SIRM	0-1.24	△	under pressure	(Bezaeva, et al., 2010; Louzada, et al., 2007, 2010)
PSD	Schist	plate impact	near SIRM	3.76, 10.1	▲		(Bezaeva, et al., 2010)
MD	Synthetic powder	hydrostatic	SIRM	0-1.24	◁	under pressure	(Bezaeva, et al., 2010; Louzada, et al., 2007, 2010)
MD	Single-crystal	hydrostatic	SIRM	0.99-12.0	◇	under pressure	(Bezaeva, et al., 2010; Louzada, et al., 2007, 2010)
MD	Single-crystal	plate impact	near SIRM	0.99-12.0	◆		(Louzada, et al., 2007, 2010)

SP = Superparamagnetic. SD = Single-domain. PSD = Pseudo-single-domain. MD = Multidomain. IRM = Isothermal remanent magnetization. SIRM = Saturation isothermal remanent magnetization. ARM = Anhysteretic remanent magnetization. TRM = Thermal remanent magnetization. NRM = Natural remanent magnetization.

References in the Table

Bezaeva, N.S., Gattacceca, J., Rochette, P., Sadykov, R.A., Trukhin, V.I., (2010). Demagnetization of terrestrial and extraterrestrial rocks under hydrostatic pressure up to 1.2 GPa, PEPI 179, 7–20, doi:10.1016/j.pepi.2010.01.004.

Bezaeva, N.S., Rochette, P., Gattacceca, J., Sadykov, R.A., Trukhin, V.I., (2007). Pressure demagnetization of the Martian crust: Ground truth from SNC meteorites, GRL 34, L23202, doi:10.1029/2007GL031501.

Borradaile, G.J., (1992). Deformation of remanent magnetism in a synthetic aggregate with hematite, Tectonophysics 206, 203-218, doi:10.1016/0040-1951(92)90377-I.

Borradaile, G.J., (1992). Experimental deformation of two-component IRM in magnetite-bearing limestone: a model for the behaviour of NRM during natural deformation, PEPI 70, 64-77, doi:10.1016/0031-9201(92)90161-N.

Borradaile, G.J., (1993). Strain and magnetic remanence, Journal of Structural Geology 15, 383-390, doi:10.1016/0191-8141(93)90134-V.

Borradaile, G.J., Jackson, M., (1993). Changes in magnetic remanence during simulated deep sedimentary burial, PEPI 77, 315-327, doi:10.1016/0031-9201(93)90106-J.

Cisowski, S.M., Dunn, J.R., Fuller, M., Wu, Y., Rose, M.F., Wasilewski, P.J., (1976). Magnetic effects of shock and their implications for lunar magnetism (II), Lunar Science Conference, 7th, Houston, Tex., March 15-19, 1976, Proceedings 3, 3299-3320.

Gattacceca, J., Boustie, M., Weiss, B.P., Rochette, P., Lima, E.A., Fong, L.E., Baudenbacher, F.J., (2006). Investigating impact demagnetization through laser impacts and SQUID microscopy, Geology 34, 333-336, doi:10.1130/G21898.1.

Gattacceca, J., Lamali, A., Rochette, P., Boustie, M., Berthe, L., (2007). The effects of explosive-driven shocks on the natural remanent magnetization and the magnetic properties of rocks, PEPI 162, 85-98, doi:10.1016/j.pepi.2007.1003.1006.

Gilder, S.A., Le Goff, M., Chervin, J.-C., (2006). Static stress demagnetization of single and multi-domain magnetite with implications for meteorite impacts, High Pressure Research 26, 539-547, doi:510.1080/08957950601092085.

Kletetschka, G., Connerney, J.E.P., Ness, N.F., Acuña, M.H., (2004). Pressure effects on martian crustal magnetization near large impact basins, MAPS 39, 1839-1848, doi:10.1111/j.1945-5100.2004.tb00079.x.

Pearce, G.W., Karson, J.A., (1981). On Pressure Demagnetization, GRL 8, 725-728, doi:10.1029/GL008i007p00725.

Pohl, J., Bleil, U., Hornemann, U., (1975). Shock Magnetization and Demagnetization of Basalt by Transient Stress up to 10 kbar, Journal of Geophysics 41, 23-41.

Rochette, P., Fillion, G., Ballou, R., Brunet, F., Ouladdiaf, B., Hood, L., (2003). High pressure magnetic transition in pyrrhotite and impact demagnetization on Mars, GRL 30, doi:10.1029/2003GL017359.